André Ricardo
Correia dos Santos
Válega

Estudo termo-reológico e estrutural de peças obtidas por microinjeção

André Ricardo Correia dos Santos Válega

Estudo termo-reológico e estrutural de peças obtidas por microinjeção

Dissertação apresentada à Universidade de Aveiro para cumprimento dos requisitos necessários à obtenção do grau de mestre em Engenharia Mecânica, realizada sob orientação científica da Professor Doutor Mónica Sandra Abrantes de Oliveira Correia, Professora Auxiliar do Departamento de Engenharia Mecânica da Universidade de Aveiro e do Professor Doutor Rui António da Silva Moreira, Professor Auxiliar do Departamento de Engenharia Mecânica da Universidade de Aveiro.

O júri / The jury

Presidente / President

Professor Doutor José Paulo Oliveira Santos
Professor Auxiliar da Universidade de Aveiro

Vogais / Committee

Professor Doutor Rui Jorge Sousa Costa de Miranda Guedes
Professor Auxiliar da Faculdade de Engenharia da Universidade do Porto

Professor Doutor Mónica Sandra Abrantes de Oliveira Correia
Professora Auxiliar da Universidade de Aveiro (orientador)

Professor Doutor Rui António da Silva Moreira
Professor Auxiliar da Universidade de Aveiro (co-orientador)

Agradecimentos / Acknowledgements

A elaboração deste trabalho não seria possivel sem a ajuda de vários docentes, amigos e colegas que estiveram constatemente presentes durante o meu percurso académico. Por isso, quero deixar-lhes o meu agradecimento pessoal, e em especial a:

Aos meus pais e avós, pelo incansável e inquestionável apoio durante toda a minha vida e em especial nesta fase.

À minha madrinha pelos sábios conselhos durante o percurso académico.

A todos os companheiros de curso, e em particular ao Bruno Barroqueiro, Carlos Oliveira, Rui Bártolo, Rui Pais e Tiago Godinho por todo o apoio e entre-ajuda durante o curso.

À Professora Doutora Mónica Oliveira, por me ter dado a oportunidade de trabalhar nesta área, por nunca ter duvidado de mim e ter sido uma fonte de motivação e incentivo constante.

Ao Professor Doutor Rui Moreira pela sua disponibilidade, conselhos certos e ajuda na análise dos dados.

À Engª Tatiana por toda a ajuda na parte experimental e nas simulações.

Aos colegas de laboratório que me integraram num grupo dinâmico e activo.

A todos os que contribuiram de forma directa ou indirecta neste trabalho.

A todos eles o meu muito obrigado.

Palavras-chave tensões residuais; microinjeção; ABS; simulação numérica; viscoelasticidade; princípio de sobreposição tempo temperatura; TTSP

Resumo

Nas últimas décadas, a miniaturização dos equipamentos eletrónicos e aparelhos mecânicos tem sido uma tendência em constante desenvolvimento. A micromoldação por injeção é uma das técnicas mais utilizadas para obtenção de microcomponents plásticos para os mais variados propósitos. Através desta técnica é possível obter microcomponentes em grandes quantidades e a baixo custo, usufruindo ainda do alto nível da automação inerente ao processo. Contudo, durante o processo de moldação são originadas tensões residuais internas nas peças moldadas, devido ao escoamento do fundido e ao arrefecimento e solidificação do plástico. Neste trabalho propõe-se uma metodologia que contempla a simulação numérica do processo de obtenção de peças plásticas por injeção juntamente com uma análise estrutural. Esta última visa levar em consideração o histórico do processamento bem como o comportamento típico de um material polimérico aquando em serviço. Desse modo, o trabalho inclui o estudo e definição do comportamento viscoelástico do material. Para tal, são abordadas também metodologias de análise do comportamento viscoelástico dos materiais. O trabalho divide-se em duas partes principais: a primeira onde são feitos ensaios DMTA para caracterização do comportamento mecânico do material e propostas metodologias de análise do mesmo através do uso do princípio de sobreposição tempo-temperatura; a segunda parte incide na obtenção das tensões residuais através da simulação numérica do processo de injecção e da simulação numérica de um ensaio de relaxação de tensões no qual o modelo viscoelástico previamente criado é inserido. Os resultados obtidos permitem concluir a adequabilidade da metodologia desenvolvida, permitindo postular a sua viabilidade na simulação do comportamento de micropeças quando em serviço.

Keywords residual stresses; micro injection; ABS; numerical simulation; viscoelasticity, time temperature superposition principle; TTSP

Abstract In recent decades, the miniaturization of electronic and mechanical equipment is a tendency in constant development. Micro-injection is one of the most used techniques for obtaining plastics micro-components for various purposes. Through this technique it is possible to obtain micro-components in large quantities and at low costs, yet taking advantage of the high level of automation inherent to the process. However, during the moulding process, residual stresses start to develop on the part, due to the melt flow and due to the cooling and solidification of the plastic. In this study a methodology that addresses the numerical simulation of the injection moulding coupled with a structural analysis is proposed. The latter takes into account the effect of residual stresses on the part and the fact that polymers are viscoelastic materials. For this purpose, methodologies to analyse viscoelastic behaviour of polymers are also proposed. This work is composed by two main parts: the first, where DMTA tests are performed to characterize the mechanical behaviour of the material and where analysis methods to handle resultant data are proposed, namely by using the principle of time-temperature superposition; the second part relates to obtaining the part residual stresses through the numerical simulation of the injection process and the numerical simulation of a stress relaxation test, in which the previously developed viscoelastic model is accounted for. The obtained results provide an insight on the adequacy of the methodology here developed to assess the durability of the injected microparts when in a duty cycle.

Contents

List of Tables

List of Figures

Chapter 1

Introduction

Nowadays one of the most common techniques to produce parts is injection moulding. According to Cefamol-National Mold Industry Association in Portugal, this technique in particular, enables the production of parts at a high rate, increasing enterprises competitivity. This important industry can supply components to world leading companies in time, thanks to the Portuguese engineers experience and know-how [1].

In the last decades components miniaturization has been a growing trend as a consequence of industry development. Microinjection allows for producing parts in very high quantities with a very low cost, thanks to the process automation level. Products obtained by microinjection may have a very distinct purpose. Automotive industry is one of the largest consumers of these micro components and uses it in many imperceptible ways. Micro components are also widely used in electrical/electronic products, in medical components or even in simple things such as gears for wrist watches.

Parts produced with the microinjection process should also ensure good mechanical characteristics such as durability, physical stability at working temperatures and even small strain, since any deformation in such a small piece can make the whole part to collapse.

In order to fulfill these criteria, it is necessary a special care when choosing the polymer which will be injected. Polymers that fulfill the criteria are usually more expensive when compared to macro injection polymers but, once the quantity used is smaller, the total price of the part is not much affected. In microinjection the used material is usually non-recycled, which implies that the mold should be very well projected in order to minimize wastes.

High precision and finishing demands causes the micro injection molds to be different from macro injection [2].

Similarly to what happens on the conventional injection molding procedures, micro injection generates internal residual stresses in the components due to numerous reasons, including: stresses induced by the melt flow or even stresses due to the pressure imposed during the polymer's cooling and solidifying. The latter are responsible for the warpage and deformation of the part if not properly controlled and may lead to a more fragile component after its extraction. In micro injection molding this effect assumes an even larger importance because of the high pressure and injection velocity needed to avoid premature polymer solidifying due to the part high surface/volume ratios. Shear stress resultant from these extreme processing conditions may lead to breakage of molecular chains and cause sliding of the polymer on the mold wall, damaging the structural in-

tegrity of the micro part. It is then noticeable the importance of the processing conditions on the component future mechanical behaviour. In fact, different processing conditions may induce different part mechanical properties due to the material distinct thermo-rheological histories. The latter may be taken into account through commercial software packages such as Autodesk Moldflow® which allow the user to simulate and assess the complete part production, from filling to cooling.

Associated to the thermo-rheological history, its induced residual stresses during processing, it is detrimental to acknowledge the material mechanical behaviour in order to postulate its durability during service. It is common knowledge that polymers are viscoelastic, nevertheless its mechanical behaviour is a consequence of its processing and therefore its thermo-rheologic history and requires further assessment.

An adequate viscoelastic model needs, therefore, to be provided and a suitable methodology needs to be developed in order to postulate the part in service behaviour.

The present work aims at the prediction of a micro part behaviour during its duty service. To accomplish the latter an hybrid methodology is proposed. Firstly, the micro-part thermo-rheological historic will be obtained through process simulation by using Autodesk Moldflow® to study part filling, packing and warpage. The latter information will be used as key input to Abaqus®, where the micro part duty service will be studied. In order to obtain an assertive prediction of the micro part duty service the adequate viscoelastic constitutive model must also be prompted to Abaqus®. To adequately model the micro-part viscoelasticity, Dynamical Mechanical Temperature Analysis(DMTA) will be carried out to establish the micro-part history at different processing conditions and hence provide insight in what concerns its mechanical behaviour under certain duty cycles.

In this research work, it is intended to develop methodologies and procedures for mechanical tests at micro scale, combining a complete structural analysis based on an injection simulation with data from mechanical tests.

The main objectives are:

- literature review on polymers constitutive models, polymer testing, viscoelasticity and polymers mechanical behavior;
- to run DMTA tests to obtain data, establishing the mechanical behaviour of micro parts at specific processing conditions;
- to develop a polymer constitutive model from the mechanical tests data using techniques such as the time temperature superposition principle;
- to assess mechanical performance of a micro component when subjected to a certain mechanical solicitation, having into account its processing history.

Chapter 2

Literature review

2.1 Viscoelasticity

Classical theory of elasticity deals with mechanical properties of elastic solids, for which, in accordance with Hooke's law, stress is always directly proportional to strain in small deformations but independent of the rate of strain. Classical theory of hydrodynamics deals with properties of viscous liquids, for which, in accordance with Newton's law, the stress is always directly proportional to the rate of strain but independent of the strain itself.

Although Hooke's law approaches the behaviour of many solids for infinitesimal strains, and that Newton's law approaches many liquids behaviour for infinitesimal rates of strains, some deviations may be observed under certain situations. These deviations may be distinguished in two:

- stress-strain relations are more complicated when finite strains are imposed on solids that can deform substantially without breaking - the so called non-Hookean deformation;
- polymeric solutions and undiluted uncrosslinked polymers may deviate from Newton's law when in steady flow with finite strain rates - Non-Newtonian flow.

Polymeric materials may present both viscous resistance to deformation and elasticity. Polymers' linear viscoelastic domain is limited to relatively small stresses. This kind of materials has characteristics between those of ideal elastics and those from ideal Newtonian fluids. A not completely solid material deforms through time when subjected to a constant stress, instead of having a constant deformation, in other word it **creeps**. When such a body is constrained at constant deformation, the stress required to hold it diminishes gradually, or **relaxes**. When an external constant stress is applied to a not completely liquid material it stores some of the input energy, instead of dissipating it all as heat during its flow and it may recover part of its deformation when the stress is removed (this is called elastic recoil) [8].

Ideal elastic solids store all supplied deformation energy whilst ideal Newtonian fluids dissipate all supplied energy (except hydrostatic state of stress) [6]. When sinusoidally oscillating stresses are applied to such bodies, the resulting strain is neither exactly in phase with the stress (as it would be for a perfectly elastic solid) or 90° out of phase (as it

would be for a perfectly viscous liquid). It is then possible to build uniaxial viscoelastic behaviour models combining solids basic physical models - springs and Newtonian fluids models - dampers [6].

In certain cases, such as vulcanized (cross-linked) rubber, flow is not possible and the material has a unique configuration assumed in the absence of deforming stresses. The viscous resistance to deformation is noticed due to the rubber's delay on a change in stress [8]. In such materials some of the energy input is stored and recovered in each cycle, and some is dissipated in the form of heat. Materials whose behaviour exhibits such characteristics are called **viscoelastic**. If both strain and rate of strain are infinitesimal and the time-dependent stress-strain relations can be described by linear differential equations with constant coefficients, **linear viscoelastic** behaviour occurs. In an experiment with these materials the ratio of stress to strain is a function of time (or frequency).

A "constitutive equation" or "rheological equation of state" relates stress, strain and their time dependence. Finite strain/strain rates produce complicated constitutive equations. On the other hand, infinitesimal strain/strain rates (corresponding to linear viscoelastic behaviour) have relatively simpler constitutive equations. Viscoelasticity's constitutive laws may be expressed through the Boltzmann Superposition principle [6].

2.2 Linear constitutive equations (simple shear)

Polymers viscoelasticity is dependant of molecular structure, modes of molecular motion, molecular weight and its distribution, temperature, concentration, chemical structure, among others.

2.2.1 Equations of change

Experimental measurements of mechanical properties relate stress and strain applied to a body. Assuming that the process is isothermal (therefore despising the equation of conservation of energy), this relation depends not only on stress-strain constitutive equation but also on equation of continuity and the equation of motion. The earlier expresses conservation of mass (Equation 2.1)

$$\frac{\partial}{\partial t}\rho = -\sum_{i=1}^{3}\frac{\partial}{\partial x_i}(\rho v_i) \tag{2.1}$$

and the latter expresses the conservation of momentum (Equation 2.2

$$\rho\left(\frac{\partial}{\partial t}v_j + \sum_{i=1}^{3} v_i\frac{\partial}{\partial x_i}v_j\right) = \sum_{i=1}^{3}\frac{\partial}{\partial x_i}\sigma_{ij} + \rho g_j \tag{2.2}$$

In these equations ρ is density, t is time, x_i are three Cartesian coordinates and v_i are the components of velocity in the respective directions of the previous coordinates. In Equation 2.2, the index j may assume successively the values $1, 2, 3$, g_j is the component of gravitational acceleration in the j direction and σ_{ij} are the appropriate components of the stress tensor. Most of the experiments are made in conditions that make both sides of Equation 2.1 be zero and so that the inertial and gravitational forces in Equation 2.2

are negligible. Here, internal states of stress and strain can be calculated from observable quantities by the constitutive equation alone [10].

2.2.2 Infinitesimal strain tensor

Like in a perfectly elastic body, viscoelastic bodies exhibit a state of deformation at a given point which can be specified by a strain tensor, representing relative changes in dimensions and angles of a small cubical element in that position. The state of stress is specified by a stress tensor which represents the forces acting on different faces of a cubical element. The rate of strain tensor describes the time derivatives of these relative dimensions and angles.

For an infinitesimal deformation, the components of the infinitesimal strain tensor, in rectangular coordinates with the three cartesian directions $(1, 2, 3)$ are:

$$\gamma_{ij} = \begin{pmatrix} 2\frac{\partial u_1}{\partial x_1} & \frac{\partial u_2}{\partial x_1} + \frac{\partial u_1}{\partial x_2} & \frac{\partial u_3}{\partial x_1} + \frac{\partial u_1}{\partial x_3} \\ \frac{\partial u_2}{\partial x_1} + \frac{\partial u_1}{\partial x_2} & 2\frac{\partial u_2}{\partial x_2} & \frac{\partial u_2}{\partial x_3} + \frac{\partial u_3}{\partial x_2} \\ \frac{\partial u_3}{\partial x_1} + \frac{\partial u_1}{\partial x_3} & \frac{\partial u_2}{\partial x_3} + \frac{\partial u_3}{\partial x_2} & 2\frac{\partial u_3}{\partial x_3} \end{pmatrix} \tag{2.3}$$

Here, x_i and u_i are the point coordinates and its displacement in the strained state ($u_i = x_i - x_i^0$), respectively. The rate of strain tensor, $\dot{\gamma}$ is similar to strain tensor with u_i replaced by v_i, the velocity of displacement [10].

2.2.3 Stress tensor

Stress components of σ_{ij} that appear in 2.2 can be represented by:

$$\sigma_{ij} = \begin{pmatrix} \sigma_{11} & \sigma_{12} & \sigma_{13} \\ \sigma_{21} & \sigma_{22} & \sigma_{23} \\ \sigma_{31} & \sigma_{32} & \sigma_{33} \end{pmatrix} \tag{2.4}$$

For a stress component σ_{ij} the first index i indicates the plane that the stress is perpendicular to and the second index j denotes the parallel direction in which the stress acts, as seen in Figure 2.1. Normal stresses σ_{ii} are usually positive for tension and negative for compression [10].

2.2.4 Constitutive equation for linear viscoelasticity (simple shear)

When deformation is homogeneous/uniform, stress and strain components do not vary with position and are independent of x_i. In case of simple shear, where two opposite faces are displaced by sliding, both tensors assume more simple forms. Assuming that the plane 13 slides in direction 1, strain tensor is given by:

$$\gamma_{ij} = \begin{pmatrix} 0 & \gamma_{12} & 0 \\ \gamma_{21} & 0 & 0 \\ 0 & 0 & 0 \end{pmatrix} \tag{2.5}$$

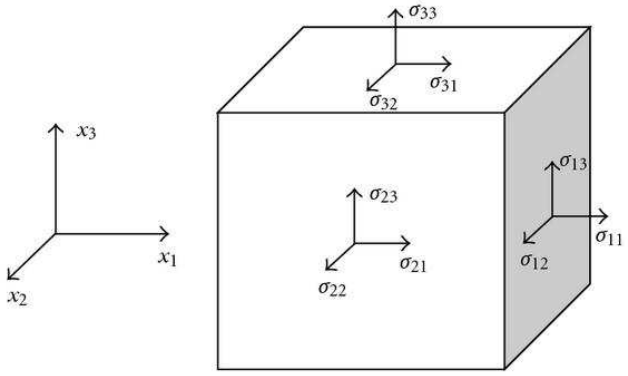

Figure 2.1: Components of the stress tensor [3]

where $\gamma_{12} = \gamma_{21} = \frac{\partial u_1}{\partial x_2} = tan(\alpha) \approx \alpha$ and stress tensor is given by:

$$\sigma_{ij} = \begin{pmatrix} -P & \sigma_{12} & 0 \\ \sigma_{21} & -P & 0 \\ 0 & 0 & -P \end{pmatrix} \tag{2.6}$$

where P is an isotropic pressure. Strain γ_{12} and stress σ_{12} are functions of time and they are related by a constitutive equation for linear viscoelasticity:

$$\sigma_{21}(t) = \int_{-\infty}^{t} G(t-t')\dot{\gamma}_{21}(t')dt' \tag{2.7}$$

where $\dot{\gamma}_{21} = \partial\gamma_{21}/\partial t$ is the shear rate, $G(t)$ is the relaxation modulus.

Strain can be expressed in terms of the history of the time derivative of the stress:

$$\gamma_{21}(t) = \int_{-\infty}^{t} J(t-t')\dot{\sigma}_{21}(t')dt' \tag{2.8}$$

where $\dot{\sigma}_{21} = \partial\sigma_{21}/\partial t$ and $J(t)$ is the creep compliance.

The equation that expresses stress in terms of the history of the strain rather than the its time derivative is:

$$\sigma_{21}(t) = -\int_{-\infty}^{t} m(t-t')\gamma_{21}(t,t')dt' \tag{2.9}$$

where m(t) is the memory function and it is equal to $-dG(t)/dt$ and $\gamma_{21}(t,t')$ is a reference state.

Knowing the shear relaxation modulus, the memory function, or the creep compliance function of a material, enables to predict its stress-strain relations as long as motions are sufficiently small or slow [10].

2.3 Mechanical models for viscoelastic behaviour

To perform calculations it is useful to have the desired viscoelastic property as an equation instead of a graph or table of data. It is then convenient to have a general form that contains sufficient parameters to fit experimental data for a wide range of polymers. This form can emulate the time or frequency dependence of the viscoelastic properties by using a mechanical model with a sufficient number of elastic elements (represented by springs) and viscous elements (represented by dashpots) [10].

2.3.1 Maxwell Model

One of the simplest models that can emulate a viscoelastic system is the Maxwell model, depicted in Figure 2.2. In this model, which is composed by a series association of one spring and one dashpot, the total deformation is equal to the sum of each of the deformations, i.e., $\varepsilon = \varepsilon_s + \varepsilon_d$.

Figure 2.2: Maxwell model - adapted from [23]

Here, if k represents spring's stiffness and μ fluid's viscosity the following equation can be written:

$$\frac{d\varepsilon}{dt} = \frac{d\varepsilon_s}{dt} + \frac{d\varepsilon_d}{dt} = \frac{1}{k}\frac{d\sigma}{dt} + \frac{\sigma}{\mu} \tag{2.10}$$

A new concept, the relaxation time of the element that can be understood as a measure at the time required for stress relaxation can be written as $\tau_i = \mu_i/k_i$ [10]. Assuming that a constant stress σ_0 acts, integrating Equation 2.10 results in the creep behaviour, obtained as:

$$\varepsilon(t) = \frac{\sigma_0}{\mu}t + C1 \tag{2.11}$$

$C1$ can be obtained from the initial condition $\varepsilon(0)$ as σ_0/k, and dividing strain by stress, creep compliance can be obtained as:

$$J(t) = \frac{t}{\mu} + \frac{1}{k} \tag{2.12}$$

Equation 2.12 suggests that creep compliance increases linearly by t/μ as can be seen in Figure 2.3.

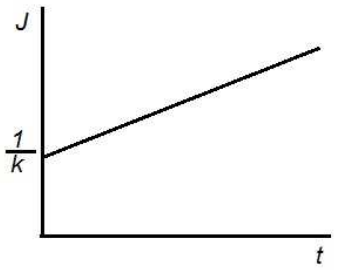

(a) Maxwell's creep compliance curve - adapted from [6]

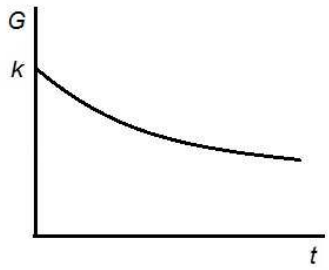

(b) Maxwell's relaxation modulus curve - adapted from [6]

Figure 2.3: Maxwell's model behaviour

However, this is not noticed experimentally and what happens is the opposite, a decrease over time, so this simple model is not good enough to represent compliance. Still, making $\varepsilon = \varepsilon_0$ and integrating 2.10 this model can predict stress as:

$$ln(\sigma) = -\frac{k}{\mu}t + C2 \tag{2.13}$$

Here, assuming that $\sigma(0) = \sigma_0$ one can write that relaxation is depicted by:

$$G(t) = k\exp(-\frac{kt}{\mu}) \tag{2.14}$$

This is concomitant with the behaviour experimentally expected [6].

2.3.2 Voigt-Kelvin Model

Another simple model to represent a viscoelastic material is the Voigt-Kelvin model. The latter is also composed by one spring and one dashpot, but this time the association is made in parallel.

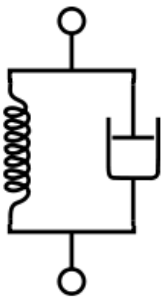

Figure 2.4: Voigt-Kelvin model - adapted from [23]

Here, the ratio between the spring and dashpot is defined as the retardation time, a measure of the time required for the extension of the spring to achieve its equilibrium length while retarded by the dashpot. In this model, creep compliance is given by:

$$J(t) = \frac{1}{k}\left[1 - e^{\frac{-kt}{\mu}}\right] \tag{2.15}$$

Still, relaxation can be written as :

$$G(t) = k \tag{2.16}$$

Similarly to the previous model, this one fails in predicting the creep compliance since it lacks the initial elastic response. Oppositely to the previous model, this one does not predict stress relaxation since $G(t)$ is given by a constant which is not time dependent and so does not change over time, as it can be seen in Figure 2.5 [6].

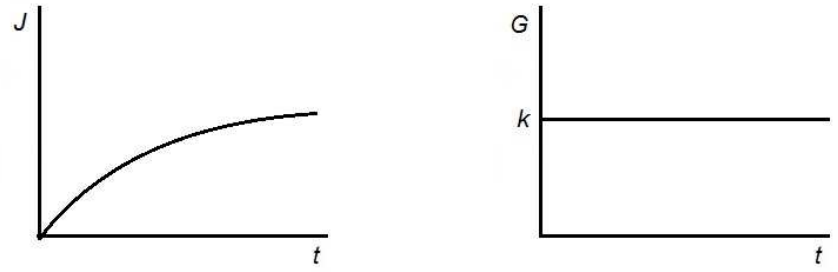

(a) Voigt-Kelvin's creep compliance curve- adapted from [6]

(b) Voigt-Kelvin's relaxation modulus curve - adapted from [6]

Figure 2.5: Voigt-Kelvin's model behaviour

2.3.3 Zener Model

There are more complex models that can emulate a viscoelastic material's behaviour. One of them is the Zener model. This model fills some flaws of previous models but it still is composed by them. It can be represented as one simple Maxwell model in parallel with one spring.

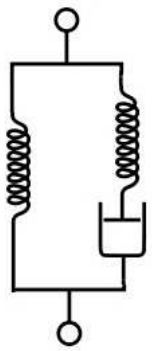

Figure 2.6: Zener model- adapted from [6]

This model states that creep compliance and relaxation are given by:

$$J(t) = \frac{1}{k_0}\left[1 - \frac{k_1}{k_0 + k_1} \cdot e^{\frac{-t}{\rho_1}}\right] \tag{2.17}$$

$$G(t) = k_0 + k_1 e^{\frac{-t}{\lambda_1}} \tag{2.18}$$

where ρ_1 and λ_1 are time constants, given by:

$$\rho_1 = \frac{\mu_1}{k_0 k_1}(k_0 + k_1) \tag{2.19}$$

$$\lambda_1 = \frac{\mu_1}{k_1} \tag{2.20}$$

Although the shapes of the curves produced by this model are similar to those obtained experimentally (Figure 2.7), it doesn't allow for a rigorous adjustment of the behaviour of polymers since time constants ρ_1 and λ_1 are insufficient. Once polymers often have a microstructural complex structure they present a continuous spectrum of time constants and there is a need of using models with enough springs and dashpots to achieve a good approximation to the polymer real behaviour [6].

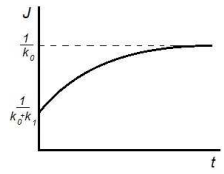

(a) Zener's creep compliance curve - adapted from [6]

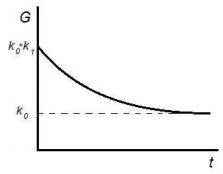

(b) Zener's relaxation modulus curve - adapted from [6]

Figure 2.7: Zener's model behaviour

Improved models

To achieve a good aproximation, more complex models which include paired or series groups of simpler models were developed, such as improved Zener models or generalized Maxwell models. The main difference between these is the addition of one element composed only by a spring as it can be seen in Zener's model [6].

Improved Zener models creep compliance and relaxation can be obtained as:

$$J(t) = \frac{1}{k_0} + \sum_{i=1}^{n} \frac{1}{k_i}\left[1 - e^{\frac{-t}{\rho_i}}\right] \quad where \quad \rho_i = \frac{\mu_i}{k_i} \tag{2.21}$$

$$G(t) = k_0 + \sum_{i=1}^{n} k_i \cdot e^{\frac{-t}{\lambda_i}} \quad where \quad \lambda_i = \frac{\mu_i}{k_i} \tag{2.22}$$

Due to this large amount of parameters, rigorous representation of viscoelastic behaviour demands an enormous experimental effort which may become time-consuming and therefore invalidating its determination [10].

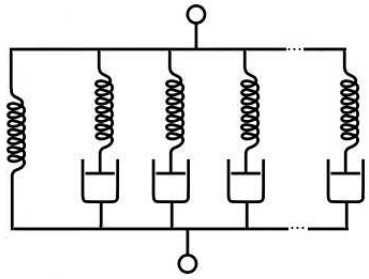

(a) Parallel association - adapted from [6]

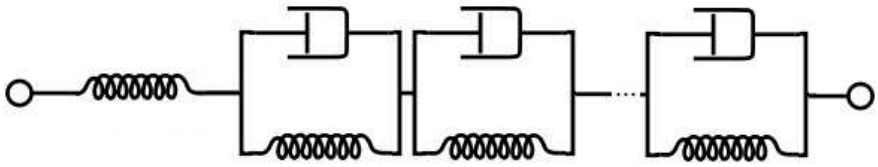

(b) Series association - adapted from [6]

Figure 2.8: Improved Zener's models

2.3.4 Viscoelastic spectra

Maxwell elements in series have the properties of a single element with $J = \sum J_i$ and $1/\mu_0 = \sum 1/\mu_i$. Voigt elements in parallel have the same properties as a single element with $G = \sum G_i$ and $\mu_0 = \sum \mu_i$. However, when more complicated models such as those presented before are used, these properties relations are not so direct.

A group of parallel Maxwell elements represents a discrete spectrum of relaxation times, each one τ_i being associated with a spectral strength k_i. In a parallel arrangement the forces are additive and viscoelastic functions such as G(t) may be obtained by summing terms equal to those in Equation 2.14, obtaining:

$$G(t) = \sum_{i=1}^{n} k_i e^{\frac{-t}{\tau_i}} \tag{2.23}$$

A group of Voigt elements in series represents a discrete spectrum of retardation times, each being associated with a spectral compliance magnitude J. In a series arrangement the strains are additive , the compliance function $J(t)$ may be obtained by summing 2.15 over all the series elements:

$$J(t) = \sum_{i=1}^{n} \mu_i \left(1 - e^{\frac{-t}{\tau_i}}\right) \tag{2.24}$$

These equations can fit relaxation and creep data with any desired degree of accuracy if n is large enough by determining the discrete spectrum of curves, each with a location τ_i and intensity k_i. Experimentally it is difficult to determine the parameters τ_i or k_i and its arbitrary choice may be enough to predict macroscopic behavior but wouldn't have enough value for theoretical interpretation. This can be avoided by analysing viscoelastic functions with continuous spectra.

If the number of elements in a generalized Maxwell model increases indefinitely, the result is a continuous spectrum, where each infinitesimal contribution to system rigidity is $Fd\tau$ and is associated with relaxation times between τ and $\tau + d\tau$. This continuous relaxation spectrum is defined as $H\ dln(\tau)$, where $H = F\tau$. In these conditions, Equation 2.23 becomes:

$$G(t) = G_e + \int_{-\infty}^{\infty} He^{\frac{-t}{\tau}} dln(\tau) \tag{2.25}$$

where G_e is a constant added to allow for a discrete contribution of the spectrum with $\tau = \infty$ for viscoelastic solids and for viscoelastic liquids it assumes value 0.

The same analogy can be established for the Voigt-Kelvin model. Here if the model is indefinitely extent it will represent a continuous spectrum of retardation times L. Equation 2.24 may be written as:

$$J(t) = J_g + \int_{-\infty}^{\infty} L\left(1 - e^{\frac{-t}{\tau_i}}\right) dln(\tau) + \frac{t}{\mu_0} \tag{2.26}$$

Here, an instantaneous compliance J_g is added to exist the possibility of a discrete contribution when $\tau = 0$. This parameter can not be determined experimentally but should be taken in account [10].

2.4 Polymeric materials

Industrial polymers consist of large molecules which are primarily covalently bonded. These molecules may arrange themselves in main chains and may present side chains, circular molecules and interconnections among them by many mechanisms.

Atoms inside molecules may interact with atoms from a different molecule. Thereby larger molecules attract each other more strongly than shorter ones. This is reflected in polymers melting points, which generally increase with increasing chain length. Hence, melting points may be a good indicator of the bond strength among molecules of the compound.

These polymer long chains are composed by small basic units called mers, which are repeated to generate the chain. The bigger the number of repeating mers, the larger the degree of polymerization of the polymer, which can be evaluated by an average number since different molecules may have different chain lengths. As the number of intermolecular attractions between mers increases, the total force of attraction and the mechanical strength of the polymer generally increases too, since mechanical failure is associated with breaking the attractive forces between the atoms in molecules. However, increasing the degree of polimerization indefinitely does not ensure an increase in strength because the chain may become so long that some parts may behave independently and can even break from the main chain. The large dimensions of these molecules are also responsible for the unique properties of polymers relatively to other materials.

Thermal energy may cause vibration of the atoms and increase atomic and molecular motions. These motions can be:

- atomic vibrations in the carbon backbone chain, which may increase the average interatomic distance and therefore the total chain length;

- vibrations perpendicular to the bond direction which can cause small vibrations in bond angles;
- rotation of the carbon atoms around the bonds causing twisting of the chain.

These vibrations can be understood as a measure of the kinetic energy which continuously changes with time. Therefore, the average interatomic distance between atoms increases with temperature.

Because bond within the chain backbone are covalent, they are of high stability and strength, and their rupture requires large amounts of energy. Forces involved in interaction with neighbouring molecules are significantly weaker and failure of a polymer is more likely to occur by breaking these connections rather than by rupturing the molecule itself [18].

There can be still connection points between linear polymers chains along their length making a cross-linked structure. When the cross-linking agent in the polymer is activated by temperatures, chemical cross links are obtained and therefore a thermoset polymer may be obtained. Physical cross-links may also occur temporarily when long molecules in linear polymers get entangle. Another phenomena that can occur is chain-branching, where a secondary chain initiates from a point on the main chain. These branch points lead to considerable differences in mechanical behaviour when comparing the same polymer with and without branching points.

Polymers chains may be of various lengths and therefore their molecular mass will also vary. Mass distribution is of importance in properties of the polymer since it will influenciate the polymer final state.

The manner in which polymers mers arrange themselves in the backbone classifies the polymer, making it a copolymer or a homopolymer. A homopolymer is a sequence of identical mers in the chain backbone, forming long equal groups. A copolymer is formed when chemical combination exists in the main chain between two or more different mers. When combination is made by groups a block copolymer is obtained. When they are disposed in any order a random copolymer is obtained.

These techniques of modifying homopolymers may also form grafts, long side chains of a second polymer chemically attached to the base polymer, or blends. By applying them, ductility or toughness of brittle homopolymers are enhanced as well as the stiffness of some rubbery polymers. Acrylonitrile-Butadiene-Styrene copolymer (ABS) is an example of a blend. In ABS the introduction of the butadiene, the rubber phase, improves the polymer impact resistance.Beyond enhancing polymers mechanical properties, these additives may also improve polymer processability and resistance to degradation [24].

2.4.1 Temperature influence on regions of viscoelastic behaviour

Thermoplastics and elastomers show very large changes in properties with temperature. Thermoplastics temperature dependence has two points of major interest. Usually polymers change from a glassy state to a rubbery state as either the temperature is raised or the time-scale of the experiment is increased. At low temperatures, in the glassy state, polymers are hard and brittle. Its stiffness relates with changes in stored elastic energy on deformation which are associated with small displacements of the molecules from equilibrium positions. Here, thermal energy is insufficient to overcome the potential barriers for rotational and translational motions of polymer molecules [21]. As the temperature

rises, the amplitude of vibrational motion becomes greater, and thermal energy becomes comparable to the potential energy barriers. Thereby, molecules can adopt conformations where they reach a minimum of free energy. These rubber-like deformations are associated with changes in the molecular conformations. This suggest that there is only one viscoelastic transition, from the glassy state to rubber. In practice, there are more relaxation transitions, as it can be seen in Figure 2.9 [24].

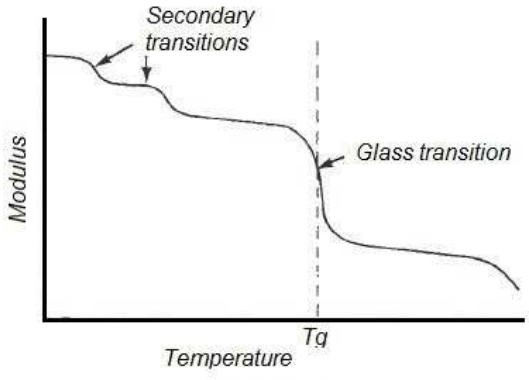

Figure 2.9: Transitions in polymer- adapted from [24]

The primary transition where the greatest change in modulus occurs is denoted T_g, and corresponds to a relaxation called α. Here the modulus decreases abruptly in the glass transition region. Glass transition should be seen as a region instead of a fixed temperature and its extent can get up to $20°C$ [24].

Beyond these regions of major importance there are other regions requiring further analysis. As the temperature is further increased the modulus reaches again a plateau. This new plateu E_2 can be seen in Figure 2.10.

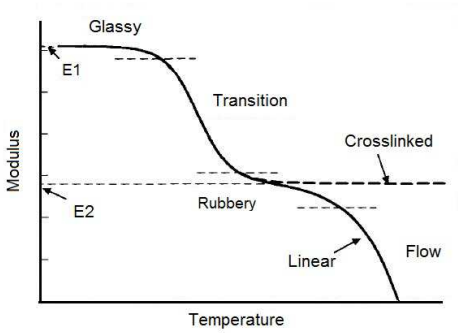

Figure 2.10: Regions of viscoelastic behaviour - adapted from [21]

Here short-range motions of the polymers occur very fast unlike the long-range motions of chains that are still restricted by the presence of strong local interactions with neighbouring chains, as Figure 2.11 exemplifies.

In case of cross-linked polymers these interactions are primary chemical bonds, known as **entanglements** in linear polymers. In the rubbery plateau segments of chains can reorient themselves relatively to each other but large translations require long times to

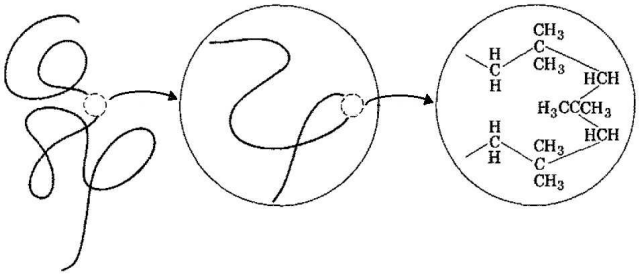

Figure 2.11: Symbolic representation of long and short range relationships in a flexible polymer molecule- adapted from [10]

occur.

In the rubbery region, linear and cross-linked polymers behave approximately but as the temperature rises this behaviour starts to differ. Because of the primary chemical bonds the changes in modulus relatively to those of the glass transition are small. Modulus only starts to decrease again significantly when temperature approaches to those where chemical degradation begins. The abrupt drop highlighted in Figure 2.10 is reached due to molecular motions caused by the increase of temperature until a state where all the molecules are able to begin to translate. These large temperatures are responsible to overcome the potential energy barriers or the break of local chain interactions which are no longer able to prevent the molecular flow [24].

2.4.2 Thermoplastics and thermosets

Polymers are usually divided in three main categories: thermoplastics, thermosets and elastomers.

When considering thermoplastics, the main chain molecules are bonded by primary covalent bonds within the chain. Secondary forces between the induced or present dipoles are responsible for the attraction between chains . Therefore, molecules are capable of individual motion and when a solid polymer is submitted to heat it can melt, being able to flow and fill a mould. This capability of being processed by injection moulding makes thermoplastics the most commonly used type of polymer.

In thermosets, covalent bonds may exist between different chains. By existing these primary bonds between different molecules, intermolecular forces are strengthened and the identification of any long single chain is very difficult if not impossible, creating a single large network instead of existing many single molecules. Since covalent bonds cannot be broken without degrading the properties of the polymer, these materials are not able to be molten by heating, but they char and decompose. Because of the referred covalent bonds these polymers are strengthened but the capability of mould filling is lost [8].

2.4.3 Amorphous and crystalline thermoplastics

Like solid materials, polymers may be classified according to their molecular structure in crystalline or amorphous.

Many polymers may form regions of cristalinity if cooled slowly from melt regions so that the long molecules can become ordered in the solid state as seen in Figure 2.12 a). The degree of crystalinity may vary because cooling from a molten state may induce imperfections caused by tangling and twisting of linear chains. Also, in order to crystalize, the molecules must have regular structure. Three dimensional juxtaposition of molecular chains may also lead to formation of crystallites, though for this to happen they have to be oriented in the same way. This way solid polymers that present a periodical tridimensional organization are called crystalline polymers and those who present regions of crystallinity are called semi-crystalline polymers [24]. These crystallites may act as crosslinks, making the rubbery plateau more pronounced in polymers with a certain degree of crystallinity than in the amorphous ones. When a polymer has a certain degree of cristalinity, regions that can be easily identified in amorphous polymers are no longer so well defined. Usually these kind of polymers manifest a significantly less fall in modulus over the glass transition temperature. It can reach up to one or two orders of magnitude when compared to amorphous polymers. Also, the change in modulus or loss factor with temperature is more gradual, what indicates a larger relaxation time spectrum. At higher temperatures crystalline regions reduce molecular mobility and so the polymer stops behaving as a rubber-like material [24]. Also, crystalline polymers exhibit a different main transition than the amorphous ones. They melt from an ordered crystal directly to a liquid. This usually happens at a region of temperatures called temperature of melting T_m. Here, the modulus drops sharply to the rubbery plateau.

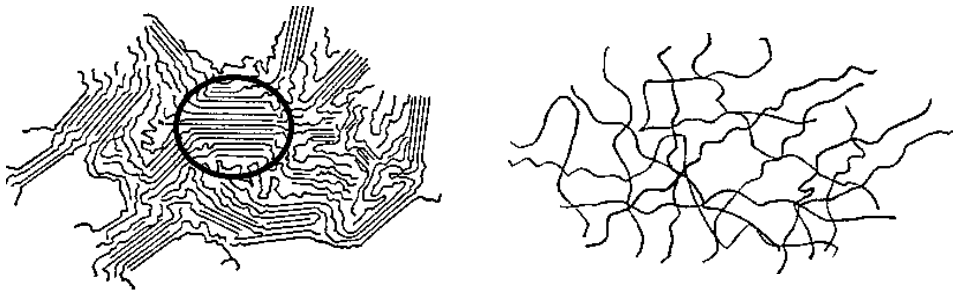

(a) Crystalline polymer structure

(b) Amorphous polymer structure

Figure 2.12: Typical polymer structure - adapted from [4]

Amorphous polymers are materials that do not have a long range periodical organization, as Figure 2.12 b) suggests. These materials may present an elastic modulus around 10^9 Pa at higher frequencies, where the viscous component is not so noticeable. When the material has high molecular mass, there is a plateau in modulus and molecular flow occurs at frequencies below $10^{-}5$ Hz. This plateau in the rubbery region can be explained due to the entanglement of molecules and the phenomena of physical crosslinking that tend to restrict molecular flow through the formation of temporary networks. At long times these entanglements tend to induce irreversible flow unlike what happens with permanent chemical cross-links (for example when a rubber is vulcanized). The modulus value in this plateau is directly proportional to the amount of these cross-links per unit of volume. In fact, lower mass samples tend to not show a rubbery plateau, passing directly from the viscoelastic region to permanent flow. In polymers with higher

molecular weight this plateau is more noticeable since it will take longer time for the chains to disentangle, increasing its length along the time axes [9]. In the glassy state, at lower temperatures, the stiffness of polymer is related to changes in stored elastic energy caused by deformation, which are explained by small displacements of molecules from their equilibrium positions. At higher temperatures, in the rubbery state, molecular chains have greater flexibility and can assume forms where the minimum free energy state can be reached. Therefore, elastic deformations are associated with changes in molecular conformations. In fact, there are several transitions in an amorphous polymer. At lower temperatures there are usually many secondary transitions, called β transitions, involving small changes in modulus. These transitions can be related to side-group motions. The largest change in modulus in this kind of polymers occurs in the glass transition range of temperature [24].

2.5 Linear time-dependent experiments (shear)

Constitutive equations describe the response of a linear viscoelastic material to various patterns of stress and strain in simple shear.

2.5.1 Stress relaxation

If a shear strain γ is imposed in a brief time period ξ by a constant rate of strain $\dot{\gamma} = \gamma/\xi$, Equation 2.7 becomes

$$\sigma(t) = \int_{t_0-\xi}^{t_0} G(t-t')\frac{\gamma}{\xi}dt' \tag{2.27}$$

where t_0 is the time when the strain imposition is complete, since the rate of strain is zero before and after the defined interval. After some mathematical simplifications, where t_0 is assumed to be zero and the time t is assumed to be much larger than the interval of application of the strain ξ, Equation 2.27 can be written as

$$\sigma(t) = \gamma G(t) \tag{2.28}$$

where $G(t)$ is the relaxation modulus. Generally a ratio of a stress to strain is called a **modulus** and for a perfectly elastic solid the shear modulus G is σ/γ. In the particular case G(t) is the shear modulus time-dependent equivalent [10].

2.5.2 Creep

When a shear stress σ is applied within a brief period and is held constant, the dependence of the strain γ on time can be obtained from Equation 2.8 on the same way as Equation 2.28 was obtained from Equation 2.27 and is given by

$$\gamma(t) = \sigma J(t) \tag{2.29}$$

Here, $J(t)$ is the creep compliance, which for a perfectly elastic solid is equal to $1/G$. However, for a viscoelastic material this is not true and $J(t) \neq \frac{1}{G(t)}$ [10].

2.5.3 Sinusoidal solicitations and dynamic experiments

Stress may be varied periodically with sinusoidal solicitations at a frequency f in cycles/sec(Hz) or $w = 2\pi f$ in radians/sec. A periodic experiment at frequency w is qualitatively equivalent to an experiment at time $t = w^{-1}$. Regarding the following constitutive equation for a sinusoidal strain:

$$\gamma = \gamma^0 sin(wt) \tag{2.30}$$

where γ^0 is the maximum amplitude strain. Calculating the derivative one can obtain:

$$\dot{\gamma} = w\gamma^0 cos(wt) \tag{2.31}$$

Substituting in Equation 2.7 and making the variable change $s = t - t'$ it can be obtained:

$$\sigma(t) = \gamma^0 \left[w \int_0^\infty G(s) sin(ws) ds \right] sin(wt) + \gamma^0 \left[w \int_0^\infty G(s) cos(ws) ds \right] cos(wt) \tag{2.32}$$

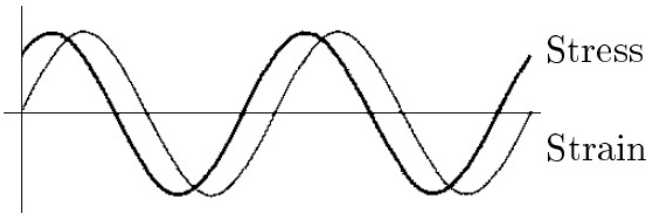

Figure 2.13: Phase lag between stress and strain - adapted from [10]

The two components of material's stress response may be distinguished as one in phase ($sin(wt)$) an one other out of phase ($cos(wt)$) with the imposed strain. This emphasises the idea that viscoelastic materials have an intermediate behaviour between ideal Newtonian fluids and ideal solids [6]. Since the quantities in brackets in Equation 2.32 are only functions of frequency and not the elapsed, Equation 2.32 can be written as:

$$\sigma = \gamma^0 (G' sin(wt) + G'' cos(wt)) \tag{2.33}$$

Here, two frequency dependant functions are defined: $G'(w)$, the shear storage modulus and $G''(w)$, the shear loss modulus. As it is a sinusoidal solicitation it is of interest to formulate the stress in an alternative form, displaying the stress amplitude $\sigma^0(w)$ and the phase angle $\delta(w)$ among stress and strain:

$$\sigma = \sigma^0 sin(wt + \delta) = \sigma^0 cos(\delta) sin(wt) + \sigma^0 sin(\delta) cos(wt) \tag{2.34}$$

Comparing equations 2.33 and 2.34 it is noticeable that:

$$G' = \frac{\sigma^0}{\gamma^0} cos(\delta) \tag{2.35}$$

$$G'' = \frac{\sigma^0}{\gamma^0} sin(\delta) \tag{2.36}$$

and a new relation can then be established, the loss factor:

$$tan(\delta) = \frac{G''}{G'} \tag{2.37}$$

When the stress and strain vary sinusoidally, they can also be described as complex numbers (refered with exponent *) and so the modulus is also a complex number given by

$$G^* = \frac{\sigma^*}{\gamma^*} = G' + iG'' \tag{2.38}$$

where the real part is the elastic/storage part and the imaginary part is the energy dissipation part as ilustrated in figure2.14 [6]:

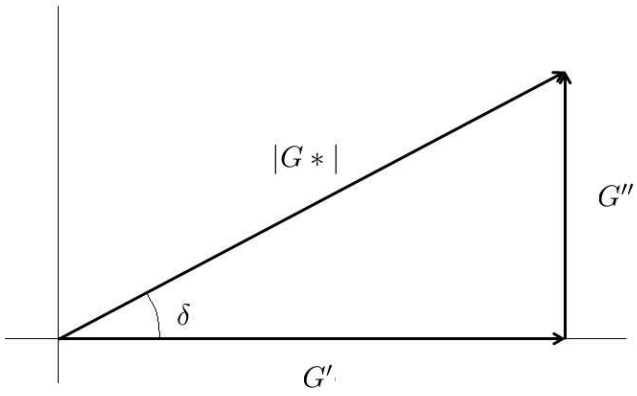

Figure 2.14: Vectorial representation of complex modulus - adapted from [10]

Here is noticeable that G' is the component of $G*$ in phase with the strain and that G'' is the component 90 out of phase. Vectorial resolution shows that :

$$|G^*| = \frac{\sigma^0}{\gamma^0} = \sqrt{G'^2 + G''^2} \tag{2.39}$$

Data from sinusoidal can also be expressed in terms of a complex compliance

$$J* = \frac{\gamma*}{\sigma*} = \frac{1}{G*} = J' - iJ'' \tag{2.40}$$

Where J', the storage compliance, is the in phase component of the stress to strain ratio to stress, whilst J'', the loss compliance is the 90 out of phase component. G' and J' are directly proportional to the average energy stored in a cycle of deformation whilst G'' and J'' are directly proportional to the average dissipation or loss of energy as heat in the same cycle.

Even if $J* = 1/G*$, individual components of module and compliance are not reciprocally related, thus can be related by [10]:

$$J' = \frac{G'}{(G'^2 + G''^2)} = \frac{\frac{1}{G'}}{1 + tan^2(\delta)} \tag{2.41}$$

$$J'' = \frac{G''}{(G'^2 + G''^2)} = \frac{\frac{1}{G''}}{1 + tan^2(\delta)^{-1}} \tag{2.42}$$

$$G' = \frac{J'}{(J'^2 + J''^2)} = \frac{\frac{1}{J'}}{1 + tan^2(\delta)} \tag{2.43}$$

$$G'' = \frac{J''}{(J'^2 + J''^2)} = \frac{\frac{1}{J''}}{1 + tan^2(\delta)^{-1}} \tag{2.44}$$

The complex module can be determined experimentally for a wide range of frequencies w through Dynamic Mechanical Analysis (DMA) or, since it may vary with temperature, through Dynamic Mechanical Thermal Analysis (DMTA). Tipically, frequencies can vary from 10^-5 to $10^8 Hz$ but below 10^-2 the experiment is time consuming and above 10^2 resonance may occur depending on the type of essay and the test specimen [6].

2.6 Dynamic and transient experiments

For understanding the viscoelastic behaviour of polymers, data are required over a wide range of time (or frequency) and temperature. This range of time may be reduced through the application of the time-temperature superposition principle as will be discussed further. Also the number of experiments may be reduced through the relations between properties. In order to cover a wide range of both time and temperature there are five main classes of experiments:

- Transient measurements: creep and stress relaxation
- Low-frequency vibrations: free oscillating methods
- High-frequency vibrations: resonance methods
- Forced vibration non-resonance methods

- Wave propagation methods

Each technique has its own range of frequency applicability as can be seen in Figure 2.15.

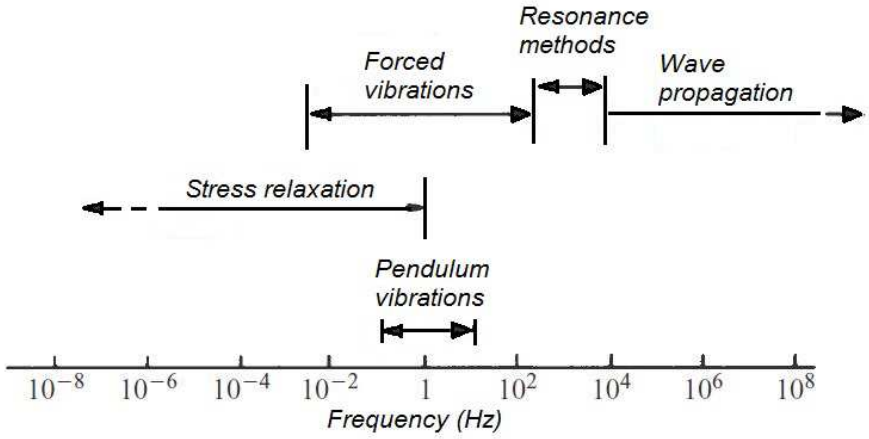

Figure 2.15: Range of frequencies for different techniques [24]

Measurements of polymers' viscoelastic behaviour are sensitive to small changes in temperature and so, a controlled temperature environment is essential. In some particular cases, such as nylon, humidity must also be controlled since they are very hygroscopic. These measurements must be done in values of strain that does not exceed one per cent since that is taken as the limit value for linear viscoelasticity [24]. Within this percentage the change in cross-section is small and hence stress cause by strain is also small. When preparing an experiment, stresses induced by the clamping forces at the end of the test specimen will induce a different state of stress from the other zones. To avoid the influence of this stress the overall length of the specimen must be 10 times its diameter or when dealing with oriented samples $10\sqrt{E/G}$ where E is the Young's modulus in the fibre direction and G the shear modulus.

Many dynamic techniques are used to cover wide ranges of frequencies, such as free oscillating pendulum methods, forced vibration techniques or DMTA. Free oscillating pendulum are simple but can only go from $10^{-}1$ to $10Hz$ and its results does not present much repeatability. On the other hand, forced vibration methods are more complex and may yield higher reproducibility and can extent the frequency range in more one decade. Nevertheless, the frequency of vibrations depends on the stiffness of the specimen, which varies with temperature [24].

However, another widely used technique is DMTA (Dynamic mechanical thermal analysis). Here, a small deformation is applied to a sample in a cyclic manner. This allows to study the materials response to stress, temperature, frequency and other values. DMTA differs from Thermomechanical Analysis (TMA) since the latter applies a constant static force to a material and evaluates the material change with temperature or in time, reporting dimentional changes, the coefficient of thermal expansion. On the ohter hand, in DMTA an oscillatory force is applied and materials response in stiffness and damping is obtained. Recent DMTA machines are also able to measure the same properties as TMA but with much more precision [24].

The amount of deformation that the sample exhibits is related to its stiffness. Thanks to high precision sensors in DMTA equipments, suchs as LVDT sensors, damping may be measured with high precision and applying this to the measured modulus, the storage modulus and loss modulus may be obtained.

Tests in DMTA may be done in various manners, such as dual cantilever, three-point bending, tension, compression or shear sandwich. Each testing mode and the geometry of the sample has its own applicability. It is dictated by the sample's physical state at the beginning of the experiment and its difficulty in applying the load. Some guidelines to preferencial geometries and types of tests are given in Table 2.1.

Table 2.1: Testing modes and specimen geometries for DMTA [17]

Sample modulus	Preferred Geometry	Sample Thickness (mm)	Free Length (mm)	Ideal Heating Rate ($^{\circ}C/min$)
10^5 to 10^{10}	Tension	0.02 to 1	2 to 10	5
10^6 to 10^{10}	Single Cantilever	1 to 2	5 to 10	3
10^6 to 10^{10}	Single Cantilever	2 to 4	10 to 15	2
10^6 to 10^{10}	Dual Cantilever	2 to 4	10 to 15	2
10^8 to 10^{12}	Three point bending	1 to 3	10 to 20	3
10^7 to 10^{11}	Three point bending	> 4	15 to 20	2
10^2 to 10^7	Simple Shear	0.5 to 2	5 to 10	≤ 2
10^2 to 10^7	Compression	0.5 to 10	15 to 20	≤ 2

DMTA latest developments allows tests to be made from temperature ranges from $-150^{\circ}C$ to $600^{\circ}C$ and frequency ranges from $10^{-}6$ to $200Hz$.

2.7 Boltzmann Superposition principle

Boltzmann Superposition Principle states that the response of a material to a given load is independent of the response of the material to any pre-imposed load so the strain response due to complex loading is the sum of the strains due to each step, as can be seen in Figure 2.16. This is only valid in linear viscoelastic region.

Considering a bar subjected to uniaxial stress variable in time, creep stress can be approximated by a series of increments $\Delta\sigma_i$ applied in times t'$_i$. The total resulting strain in t>t'$_n$ is given by Equation 2.45.

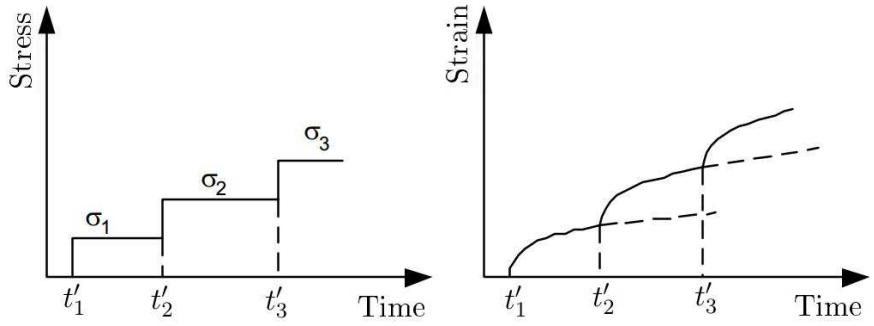

Figure 2.16: Boltzmann superposition principle - adapted from [6]

$$\varepsilon(t) = \Delta\sigma_1 J(t - t'_1) + \Delta\sigma_2 J(t - t'_2) + ... + \Delta\sigma_n J(t - t'_n) \tag{2.45}$$

where $J(t)$ is the Compliance function.

When the number of increments tends to infinity, Boltzmann Superposition Integral is obtained:

$$\varepsilon(t) = \int_{-\infty}^{t} J(t - t') \frac{d\sigma(t')}{dt'} dt' \quad where \quad J(t - t') = 0 \quad if \quad t < t' \tag{2.46}$$

$$\sigma_i(t) = \int_{-\infty}^{t} G(t - t') \frac{d\varepsilon(t')}{dt'} dt' \quad where \quad G(t - t') = 0 \quad if \quad t < t' \tag{2.47}$$

At time t'_1 stress σ_1 is applied and the strain induced can be given by

$$\varepsilon_1(t) = \sigma_1 J(t) \tag{2.48}$$

According to linear viscoelasticity $J(t)$ remains equal for all stresses in a given time. If stresses increases by $\sigma_2 - \sigma_1$ at time t'_2 the strain increase is given by

$$\varepsilon_2(t) = J(t - t'_2)(\sigma_2 - \sigma_1) \tag{2.49}$$

Also, if stress increment $\sigma_3 - \sigma_2$ is applied, the strain increase is

$$\varepsilon_3(t) = J(t - t'_3)(\sigma_3 - \sigma_2) \tag{2.50}$$

Further strains caused by stress increments, which can be either positive or negative, are added to give Equation 2.45 [6].

2.8 Time temperature superposition principle (TTSP)

The temperature dependence of polymer properties is of major importance since either polymers and elastomers present changes in their mechanical properties with changing of temperature. Polymeric parts should be projected so that creep and relaxation phenomena are slow, preferentially taking several years, albeit they can not be neglected. Hence, experimental procedures to obtain creep compliance and relaxation modulus data should also be long enough, what is not acceptable since it would be time consuming. Short time tests are then made and the results are extrapolated to working conditions. Using the time temperature superposition principle it is possible to reduce testing time by replacing it with shorter experiments at higher temperatures, since an increase in temperature accelerates molecular motions. This principle also allows to obtain a molecular interpretation of the viscoelastic behaviour since generally polymers change from glass-like to rubber-like behaviour as the temperature rises or the time scale is increased [8],[18].

TTSP principle is based on the hypotheses that viscoelastic materials have a simple rheological behavior, i.e. that every property has the same dependency of time [6].

If P designates any viscoelastic property, time temperature superposition principle states that:

$$P(t,T) = P(t_r,T_r) \tag{2.51}$$

where T_r is the reference temperature at which the properties are desired and t_r is the reduced time, given by:

$$t_r = \frac{t}{\alpha_T(T)} \tag{2.52}$$

in which intervenes the shifting factor $\alpha_T(T)$. The same can be written in frequency:

$$P(w,T) = P(w_r,T_r) \quad where \quad w_r = w\alpha_T(T) \tag{2.53}$$

The implementation of this principle requires choosing a reference temperature as well as obtaining curves for the desired property to be measured at several temperatures. It is then possible to obtain a **master curve** through shifting measured properties at each temperature by their respective shifting factors, in the time scale. This master curve may then serve as the basis to the prediction of the polymer behaviour in other situations, since by shifting the isothermals, the time scale is expanded and one can extrapolate the behaviour through longer times. Experimental calculation of the factor $\alpha_T(T)$ is essential for the application of the TTSP since these are the values to be applied to shift the isothermals horizontally.

While making master curves, variables having units of time (or reciprocal) are subject to horizontal shifts α_T while units of stress (or reciprocal) are subject to vertical shifts b_T, both temperature dependent.

When all retardation and relaxation mechanisms have the same temperature dependence as well as stress magnitudes at all times, the material can be said as thermorheologically simple. This can be noted when building a master curve if, on a double logarithmic plot of viscoelastic functions, these can be superimposed by shifting them only horizontally with the factor previously mentioned α_t. This may indicate if the dependence of

temperature is the same and if the material is considered thermorheologically simple [16]. Some authors assume that stress magnitudes are proportional to the product of the density and temperature. So the vertical shift factor may be calculated by [7]

$$b_T = \frac{T_0 \rho_0}{T \rho} \tag{2.54}$$

Another way to determine the necessity to include a vertical shift (independent of time or frequency shift), is to find the horizontal shift of loss angle necessary to superimpose on a loss angle versus $log(|G^*|)$ plot, called a van Gurp-Palmen plot [14].

2.8.1 Molecular interpretations of time-temperature equivalence

Site model theory

This theory states that there are two regions, separated by an equilibrium free energy difference $\Delta G_1 - \Delta G_2$, where each of the terms are the barrier heights per mole as Figure 2.17 shows. Also, this model is based on the transition probabilty for a jump from site 1 to site 2 when a stress is applied and a change of populations in both sites occurs [24].

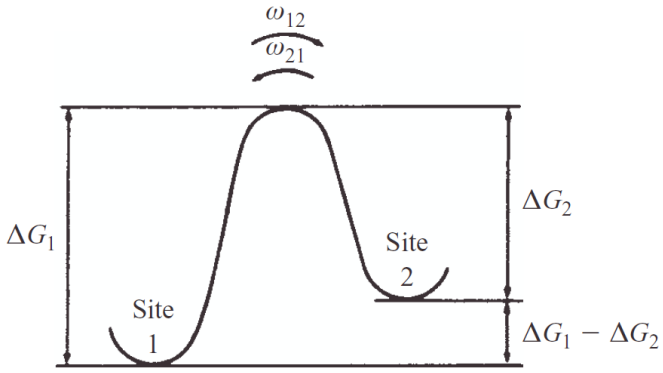

Figure 2.17: Two-site model - adapted from [24]

After some assumptions and mathematical deductions it can be stated that the frequency of molecular conformational changes depends on the barrier height ΔG_2 and not on the difference between sites, as it can be seen in Equation 2.55 . [24]

$$\nu = \frac{A'}{2\pi} e^{\frac{-\Delta G_2}{RT}} \tag{2.55}$$

Here, A' is a constant. This equation can be rewritten as :

$$\nu = \nu_0 e^{\frac{-\Delta H}{RT}} \quad where \quad \nu_0 = \frac{A"}{2\pi} e^{\frac{\Delta S}{R}} \tag{2.56}$$

Here, ΔS is the number of species per unit volume. Equation 2.56 shows that temperature affects the frequency of molecular jumps mostly by the activation energy ΔH.

Solving equation 2.56 in order to ΔH, the **Arrhenius equation** may be obtained:

$$\Delta H = -R \left[\frac{\partial (ln\nu)}{\partial (1/T)} \right] \tag{2.57}$$

This equation may be used to obtain the shift factor at temperatures inferior to glass transition temperature and allows one to superimpose curves evaluated at different temperatures [6].

$$\log(\alpha_T) = \frac{\Delta H}{R}\left\{\frac{1}{T_2} - \frac{1}{T_1}\right\} \tag{2.58}$$

The activation energy for the process can then be obtained by plotting $log(\alpha_T)$ versus the reciprocal of the temperature. It must be noted that this model may only be applied when the activation energy is constant since activation energy will be evaluated from the line's slope. Also, the temperature dependence of the glass transition relaxation behaviour is not supported by a constant activation energy model, albeit when this seems to happen it may be due to the limited range of experimental frequencies available.

William-Landel-Ferry (WLF)

One other way of calculating the shift factor for composing a master curve is the WLF equation:

$$\log(\alpha_T) = \frac{C_1(T - T_s)}{C_2 + (T - T_s)} \tag{2.59}$$

Here C_1 and C_2 are constants and they may be assumed as $C_1 = 8.86$ and $C_2 = 101.6$ when T_s, the reference temperature, is $T_s = T_g + 50°C$ for a large group of amorphous polymers. The WLF equation may be applied in a temperature range of T_g until $T_g + 100$ for this group of polymers [6].

WLF equation has a theoretical basis in terms of free volume. To understand it Equation 2.60 may be rewritten in terms of a dilatometric transition temperature :

$$\log(\alpha_T) = \frac{C_1^g(T - T_g)}{C_2^g + (T - T_g)} \tag{2.60}$$

where $T_g = T_s - 50°C$ and C_1^g and C_2^g are new constants. As Figure 2.18 shows, the total volume of the polymer is the sum of the occupied volume (molecular volume of the molecules) and the free volume (the amount of holes or voids). It is a topic of discussion that the occupied volume increases with temperature uniformly. Also, Figure 2.18 shows a sudden grow in the total volume line at T_g which suggest an expansion in free volume.

This may be explained by the start of certain molecular processes that control the viscoelastic behaviour at T_g. This brings another significance to T_g beyond the fact that T_g is the temperature when those molecular processes time scale may start to be compared with the measuring time-scale. Generally it can be assumed that free volume is constant up to T_g and then it increases linearly with temperature [24]. The classic method for the experimental determination of the glass transition temperature is dilatometry and may identify the temperature at which the change in slope occurs . Since dilamometric methods reveal to be complex in practice other methods are commonly used, such as the displacement methods or differential scanning calorimetry. The success of the first depends on the confining fluid chosen since it can not be absorbed by the polymer or undergo phase transitions. DSC (differential scanning calorimetry) registers discontinuities or peaks in heat capacity, which is observed at T_g.

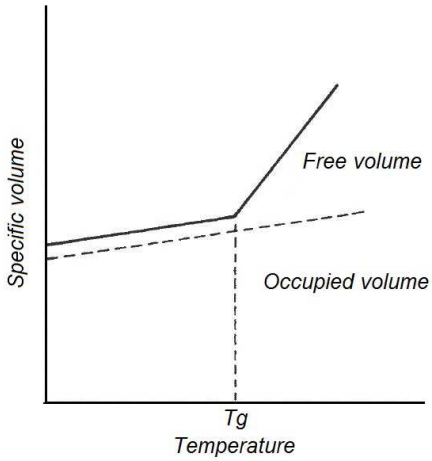

Figure 2.18: Specific volume versus temperature for a typical amorphous polymer-adapted from [24]

One criterion to the applicability of the reduced variables is the exact matching of the shapes of adjacent curves obtained experimentally. Two others are :

- the same values of α_T must superimpose all the viscoelastic functions;
- the temperature dependence of α_T must have a reasonable form, consistent with the experience.

Ferry [10] showed that it is possible to superimpose storage compliance and loss compliance with the same α_T values, forming a smooth curve. However, in the loss compliance data obtained at higher frequencies presented slight anomalies.

Even though this time temperature superimposal technique reveals of great utility it must be used very carefull. In a single investigation dynamic measurements usually do not extend over more than three decades of logarithmic frequency, nor transient measurements extend over more than six decades. Therefore, prediction of viscoelastic properties at frequencies distant from those obtained experimentally must be reasonably since small errors calculating $log(\alpha_T)$ may be accumulated and take properties to frequencies that are not correct [10].

2.8.2 Time temperature supeposition principle failure

Time temperature superposition principle is not always applicable and may not hold for many cases. For **amorphous polymers** at temperatures bellow T_g shift factors can not be obtained by the WLF equation due to the fact that in this region the rearrangement of the molecular segments within the available free volume does not contribute to the flow [9].

In case of **semicrystalline polymers**, generally this principle is less valuable. This can be explained due to the fact that semicrystalline polymers have a structure that is quite sensitive to changes in temperature and they are linearly viscoelastic only for low strain levels. WLF equation can not always be applied successfully to these polymers. Sometimes the construction of a master curve is not possible at all. In some specific

cases TTSP is possible but only for some ranges of temperature where viscoelasticity requirements are not transposed. Master relaxation curves of a semicrystalline polymer do not present the significant changes in slope that amorphous polymers do, even in the T_g zone. This may be due to the cross-linking effects of the crystallites which cause a reduction in segmental mobility. Here, T_g region will be more noticeable as fewer crystallite inclusions the polymer has [9].

Many other reasons why the TTSP may fail are conceivable, like the occurrence of more than one relaxation mechanism with distinct temperature dependence. In the vicinity of T_g both energetically and entropic induced relaxations take place and generally TTSP may not hold. Also materials with changes during the measurement time-scale will not obey TTSP [14].

Heterogeneous polymeric materials like **polymeric blends** components will generally manifest a different rheologic temperature dependence. In fact, these materials viscoelastic properties are rather complicated since many relaxation mechanisms may occur in temperature regions which are close, preventing the application of the TTSP. At temperatures where only one relaxation mechanism is active, this principle may be applied more easily. This way, grafts and blends may be expected to not obey the time temperature superposition principle.

Different groups of blends may be distinguished. **Homogeneous** polymeric materials with a distribution of chain lengths are the simplest class of blends. Generally the chain length will not influence the relaxation mechanism and there is no influence of chain length on activation energy. Branched polymers may constitute a separate class since they can be considered blends with various amounts of branching. Higher levels of branching are found on longer chains, and these are responsible for the longest relaxation times. This branching effect may affect temperature sensivity and an inhomogeneous branching distribution may lead to failure of TTSP.

Some polymers may be mixed forming a **miscible blend**, and are thought to have the same temperature dependence. Measurements on PEO/PMMA showed that TTSP fails and it can be due to the fact that each component retain their own temperature sensitivity. Only when temperature sensitivities of both components are similar (close T_g) TTSP is applicable.

Similarly to what happens to miscible blends, **immiscible blends** do not obey to TTSP. However, like in miscible blends, some cases of TTSP applicability are known. This can be due to the fact that activation energies are close. Since the success of TTSP is commonly evaluated visually, samples from the same polymer may yield good results when measured with one technique and bad results when measured with a different one. Failure of TTSP can be due to the fact that the relaxation time of one of the components falls outside of the experimental range of time. Also, interfacial effects can be seen as a relaxation mechanism with temperature dependence and can contribute to failure of TTSP [14].

However, in many cases TTSP still appears to be applicable. Examples of miscible blends where TTSP holds can be PS/PVME, SAN/SMA, PMMA/PVDF. For immiscible blends, TTSP revealed to be applicable in ABS, PS/PC, HDPE/LDPE, PE/PP [14]. Still, this principle was successfully applied on styrene-butadiene filled copolymers (in the primary transition region) and on poly(ethylene-g-styrene), which is a graft polymer, semicrystalline and heterogeneous. Styrene-based ionomers may behave has simple materials. In fact, when a polymer has a low content of these ions, the material behaves

has a simple material, whilst when contents are higher TTSP is not applicable [9].

Failure of TTSP can indicate several things:

- thermal instability of material at elevated temperatures;
- only certain regions of the experiment are able to be superposed;
- different temperature phenomena may occur such as the influence of interfacial stresses or the existence of an equilibrium modulus.

The latter item effects are elastic and therefore may only manifest in the storage modulus. This way, shifting G' and G'' may become an indicator of the existence of either elastic or frictional forces. An example of a miscible blend in which TTSP fails is PEO/PMMA, where the shifting of G' is possible but G'' is not shiftable [14].

Chapter 3

Polymer viscoelastic behaviour assessment

The present work focuses on assessing the viscoelastic behaviour of microparts. To obtain these microparts, studies were carried to estimate the best processing conditions and consequently the processing parameters. Zhil'tsova *et al.* [26], studied the influence of mesh discretization on the polymer flow behaviour in microcavities. Mesh discretization revealed to be of major importance since an increase in mesh density makes the analysis more representative of reality whilst a coarser mesh may not produce reliable results. Also, a more refined mesh will need more computational resources, increasing the time of simulation. Additionally when simulating the injection of microparts the injection assumptions may not be applicable in the same manner they are for macro parts. This study also allowed to determine the reliability of the injection simulation results by comparing them with microparts obtained experimentally. The study has established the comparison by analysing the formation of welding lines. The best results were achieved when using an external module for mesh generation, (Hypermesh® from Altair HyperWorks10®). This study highlighted the importance of the mesh type and refinement in microparts [26].

Ideal processing conditions were studied using the Moldflow® software. This study allowed one to predict some process specificities such as the fill time, temperature at flow front and the micropart warpage as it can be seen in figures 3.1-3.3.

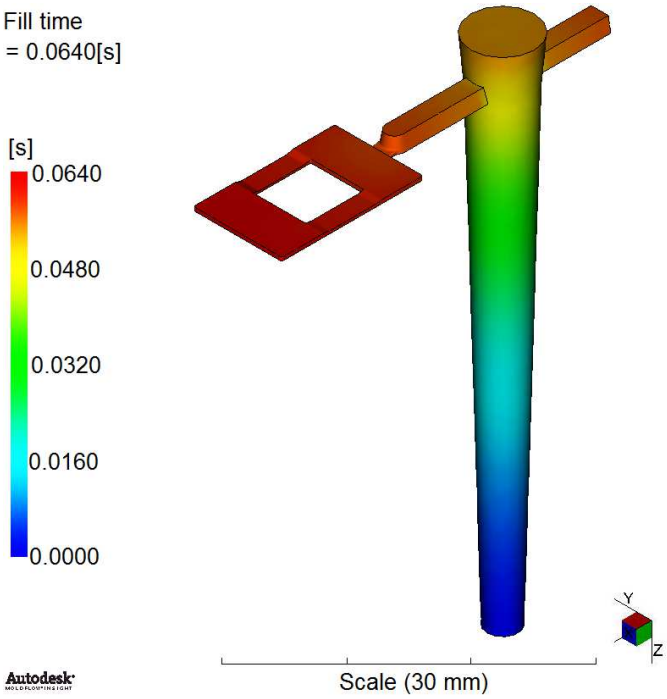

Figure 3.1: Moldflow® fill time prediction

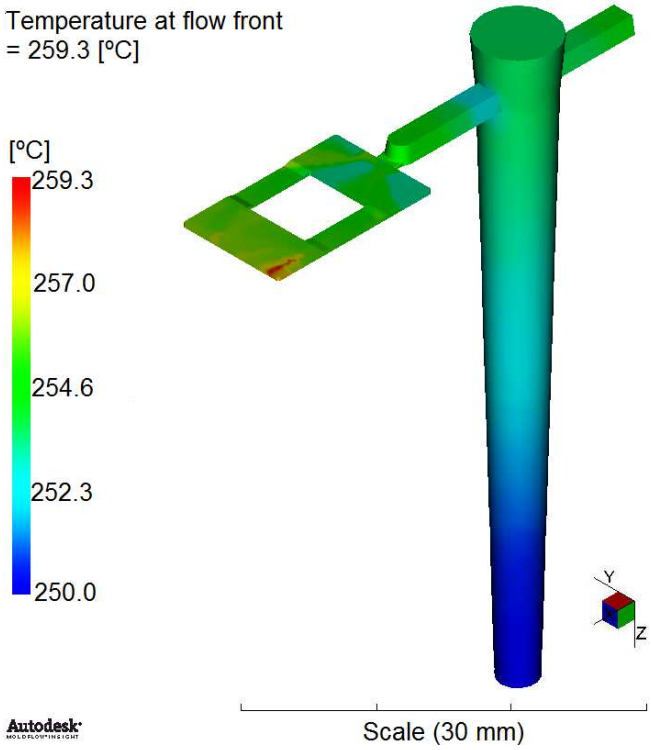

Figure 3.2: Moldflow® temperature at flow front prediction

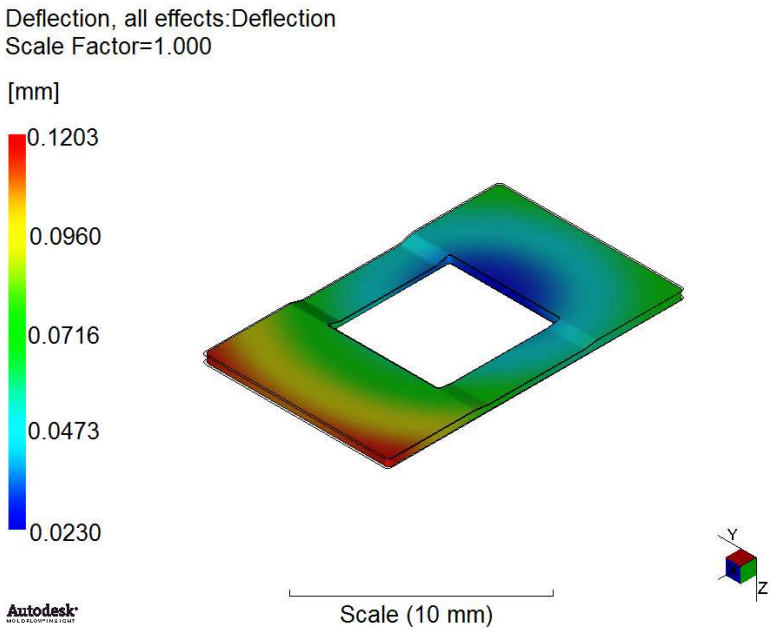

Figure 3.3: Moldflow® micropart warpage prediction

It can be seen in the previous figures that it is necessary a small amount of time, about 0.06s, to completely fill the micropart. An increase in the temperature of the flow front as it can be seen due to the fact that such small dimensions allied to the fast injection velocities tend to develop high shear rates during the injection, increasing the temperature as can be seen in the polymer flow. The greater rise in temperature can be noted in the micropart, where the polymer has to flow through a region with reduced thickness.

The study of the process (numerical) has enabled the establishment of the ideal processing conditions. Microparts were injected in a Boy 12 micro injection moulding machine (courtesy of Polymers Engineering Department of University of Minho), according to numerical simulations specifications, as presented in Table 3.1.

Table 3.1: Micropart processing conditions

Thickness [μm]	Mold Temperature[$^{\circ}C$]	Melt Temperature [$^{\circ}C$]	Cooling time [s]
200 & 300	75	250	20

The complete feeding system and micropart can be seen in figures 3.4a and 3.4b, where dotted lines represent the cutting layout to produce the specimens.

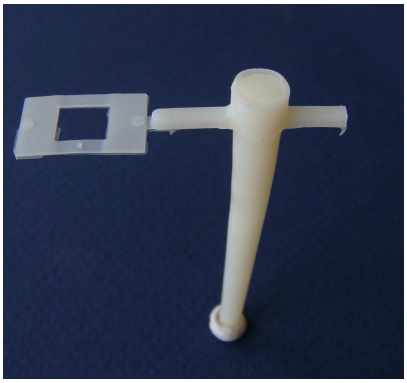

(a) Micropart and feeding system

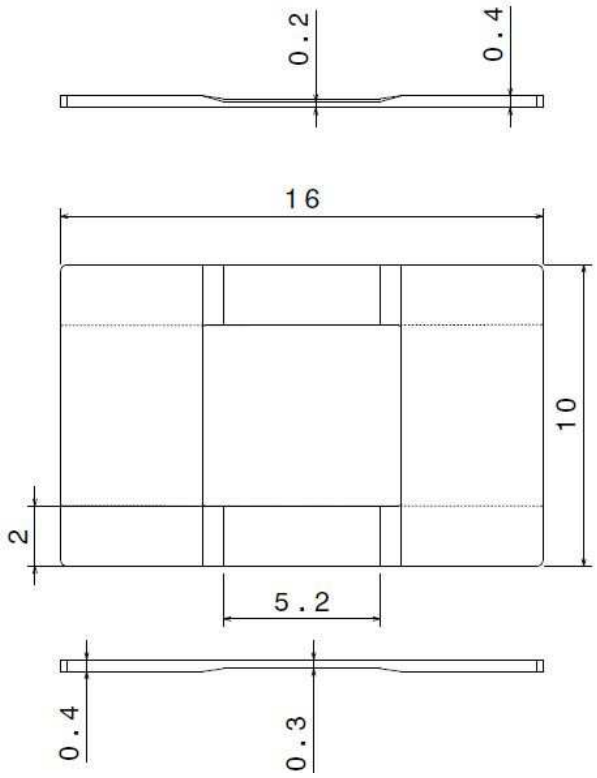

(b) Micropart dimensions [mm]

Figure 3.4: Micropart

Once obtained the microparts, DMTA tests were carried out in order to assess the mechanical properties of the polymer. These tests allowed one to obtain properties such as the time-dependent relaxation modulus and its components. The latter being: storage modulus, loss modulus and the loss factor, commonly denoted as $tg(\delta)$. The DMTA machine used was a Triton Technology TTDMA Dynamic Mechanical Analyser, courtesy of Polymers' Engineering Department of University of Minho and it is represented in Figure 3.5.

Samples were cut from the micropart including the $200\mu m$ or the $300\mu m$ zones, as Figure 3.6b suggests. Since all the sample's thickness is in the order of microns, tension configuration was considered the most appropriate test mode as the Table 2.1 suggests. Hence, the machine was set up for tension tests and the testing specimens were mounted perpendicularly to the clamps, as it can be seen from figure 3.6.

DMTA tests were performed on each sample at 16 different frequencies, equally spaced from 0.01 to 10 Hz over the temperature range of 30 to $75°C$ at intervals of $5°C$. This process was repeated for groups of 3 samples with the same processing conditions. Relaxation tests were carried imposing a displacement of $20\mu m$ which guarantees that the experiment is performed within the viscoelasticity domain of 1% of strain.

In order to estimate long-term life of the material, a Matlab® application was developed to apply the time temperature superposition principle (TTSP) to the data. The application was created to read data from the DMTA machine generated file and produce the master curves automatically. Furthermore, it intends to remove ambiguity related to

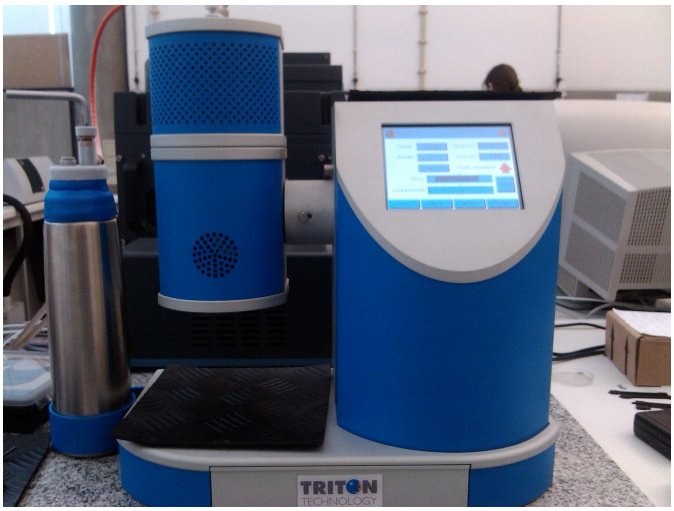

Figure 3.5: Triton Technology TTDMA Dynamic Mechanical Analyser

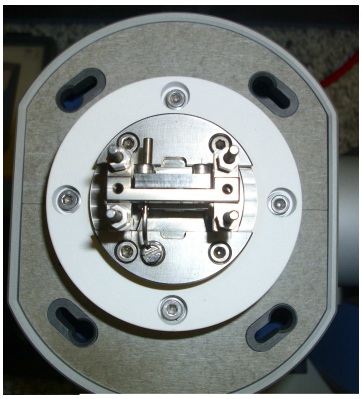

(a) Upper view

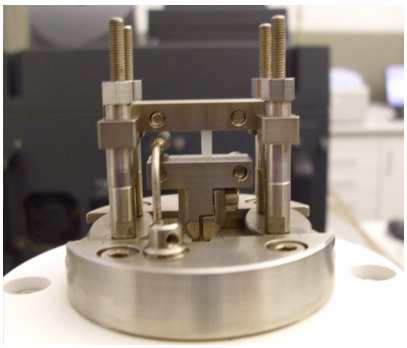

(b) Front view

Figure 3.6: Sample mounting

manual shifting processes, yielding always the same master curve as result.

The sequence followed by the application can be depicted from Figure 3.7.

DMTA data is received via a single ".xls" file where temperatures, frequencies and modulus data are presented. Data for assessing eventual problems during the experiment are also part of the file, nevertheless it is here discarded.

The developed application was programmed to sort out only the important data for the analysis and prepare it without any further user interaction.

200 and 300 μm microparts

With this set of experimental data separated, the program is now ready to let the user decide upon the thermorehological state of the material. To do so, the application yields two graphics, the Cole-Cole plot and a van Gurp Palmen plot. The analysis of the time temperature superposition principle for this material was done using a Cole-Cole plot, ($E''(w)$ vs $E'(w)$), as it can be seen in figures 3.8 and 3.9.

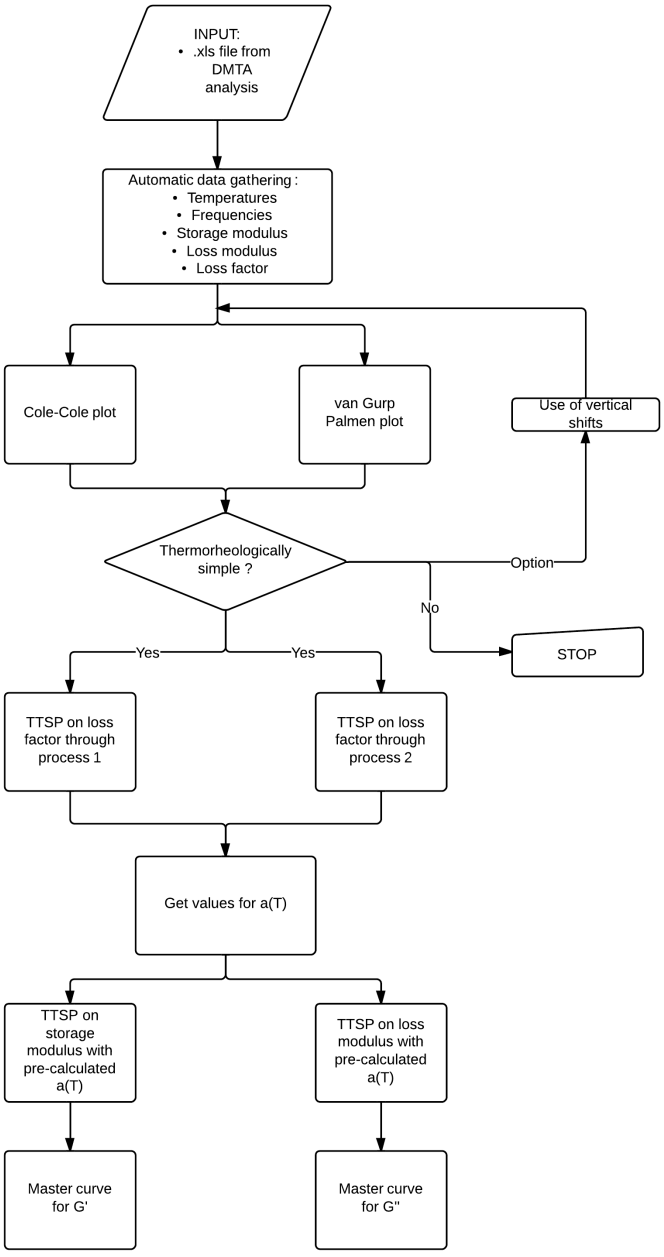

Figure 3.7: Matlab application flowchart

According to Macaubas and Demarquete [15] and Guedes [13], a material can be considered thermorheologically simple when the behaviour of the Cole-Cole plot is temperature independent.

Another way of validating the applicability of the TTSP is via the analysis of van

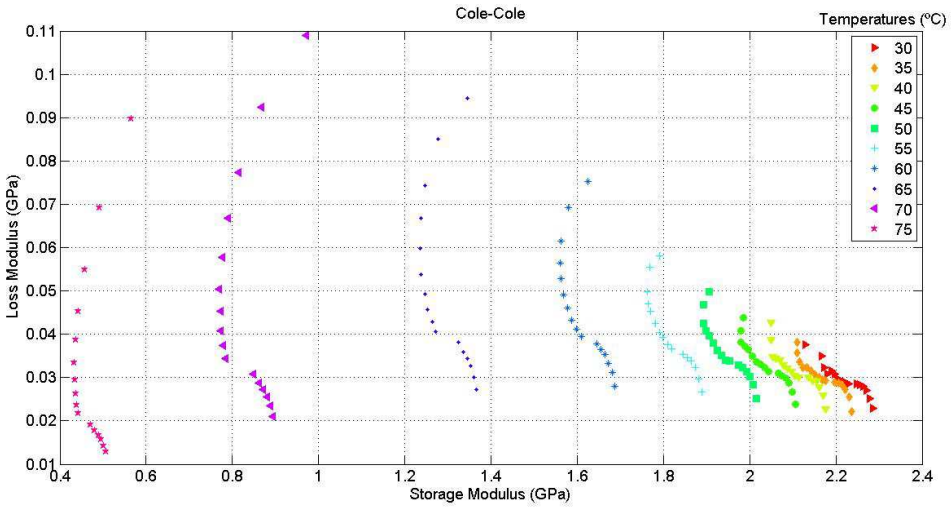

Figure 3.8: Cole-Cole plot for 200 μm ABS microparts

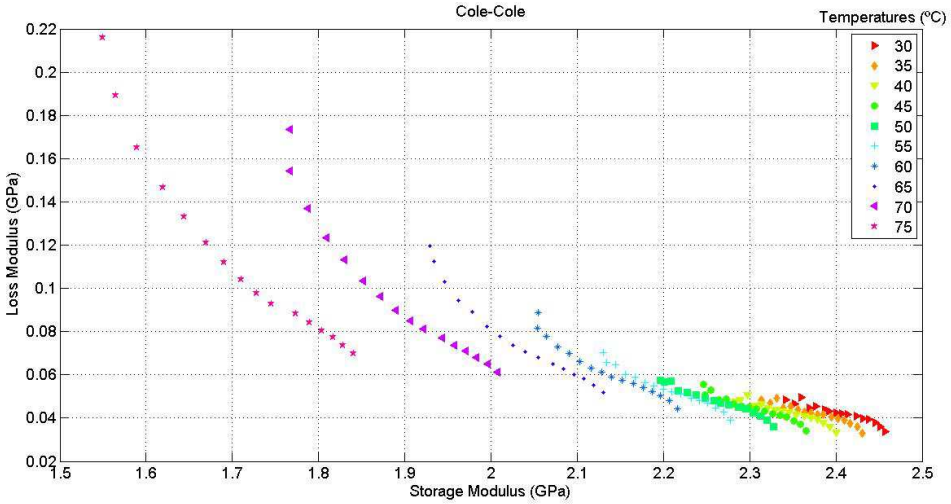

Figure 3.9: Cole-Cole plot for 300 μm ABS microparts

Gurp and Palmen[7][13][14]. This method plots the phase angle δ versus the absolute value of the complex modulus, $|G^*|$. This manner of plotting eliminates the effect of shifting along the frequency axis and yields temperature independent curves when TTSP is applicable. Moreover, this method may show directly the necessity of vertical shifting, which can not be seen in a Cole-Cole plot. van Gurp and Palmen [14] found out that for a long-chained EDPM (ethylene propylene diene monomer, M-class), failure of TTSP was clearly seen in a van Gurp Palmen plot, since a single curve was not obtained. Instead of that, a set of curves with vertical gaps between them was observed. Applying this technique to the experimental data, results in the plot that can be depicted from figures 3.10 and 3.11.

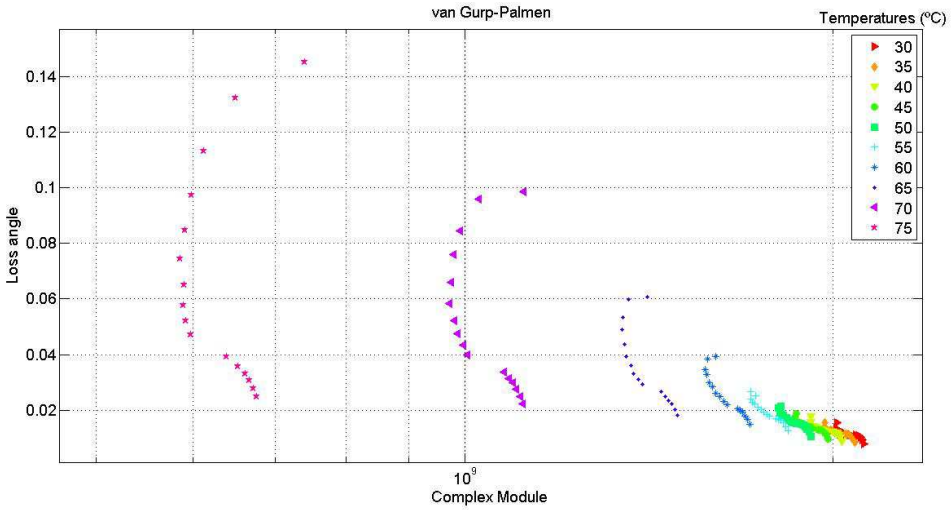

Figure 3.10: van Gurp Palmen plot for 200 μm ABS microparts

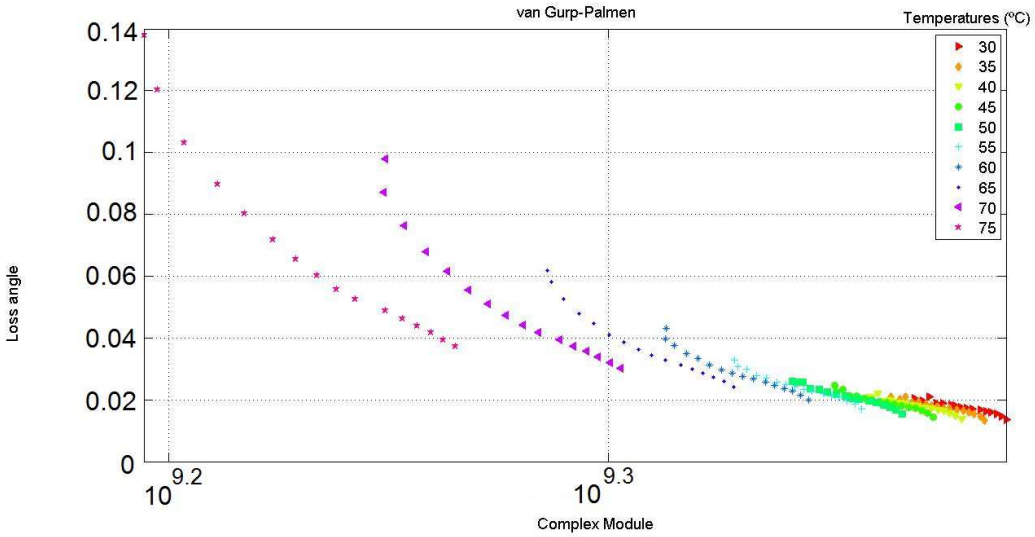

Figure 3.11: van Gurp Palmen plot for 300 μm ABS microparts

Cole-Cole plots suggest for both specimens that the behaviour seems to be temperature dependent, i.e., horizontal and a vertical shifts are necessary to obtain a single curve. van Gurp Palmen plots show that a unique single curve is not obtained for both microparts what can suggest that TTSP may not be applicable. However, in the temperature range from 30 to 55 $^{\circ}C$ a single curve tends to form but with some vertical and horizontal gaps between them.

In an attempt to obtain superposition, the vertical shift factor was included. The application also enables to use the effect of vertical shifts. For that, data containing the specific volume variation with temperature is required as input. According to Moldflow® database, the polymer's density varies with temperature as presented in figure 3.12.

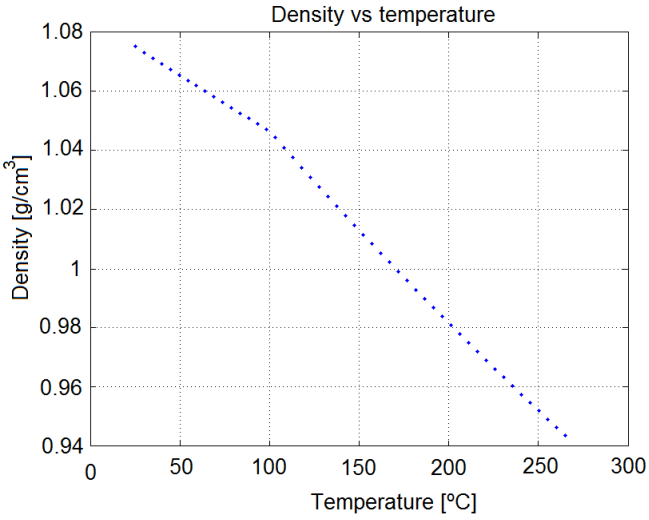

Figure 3.12: Density versus temperature plot for ABS

The vertical shift factor can then be calculated by equation (1.54). However, after obtaining shift factors from superposition of the loss factor, a single master curve for loss and storage moduli could not be obtained, even with the previous application of the vertical shift factor as figures 3.13 and 3.14 show for $200\mu m$ and 3.15 and 3.16 show for $300\mu m$. Analysing the reduced loss modulus it is possible to see that superposition is possible until $60°C$ as the Cole-Cole analysis revealed.

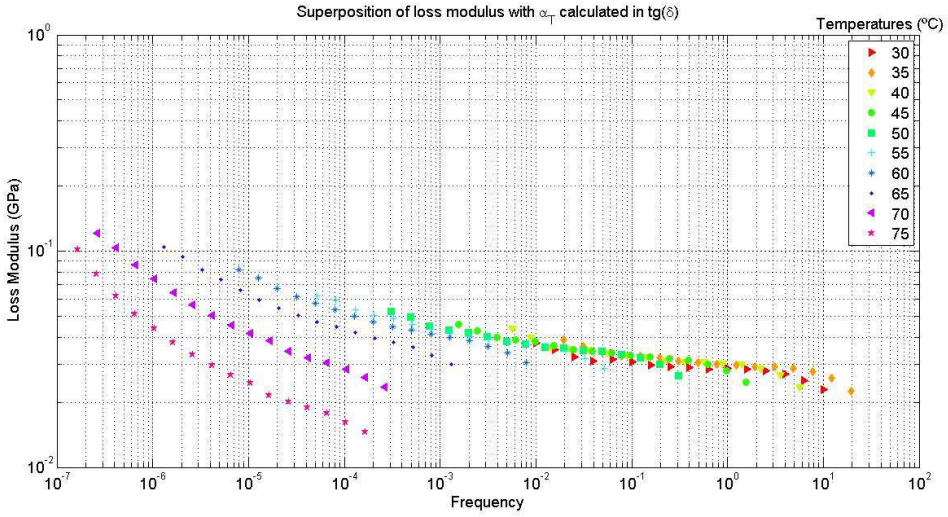

Figure 3.13: Loss modulus superposition for 200 μm ABS microparts with vertical shifting

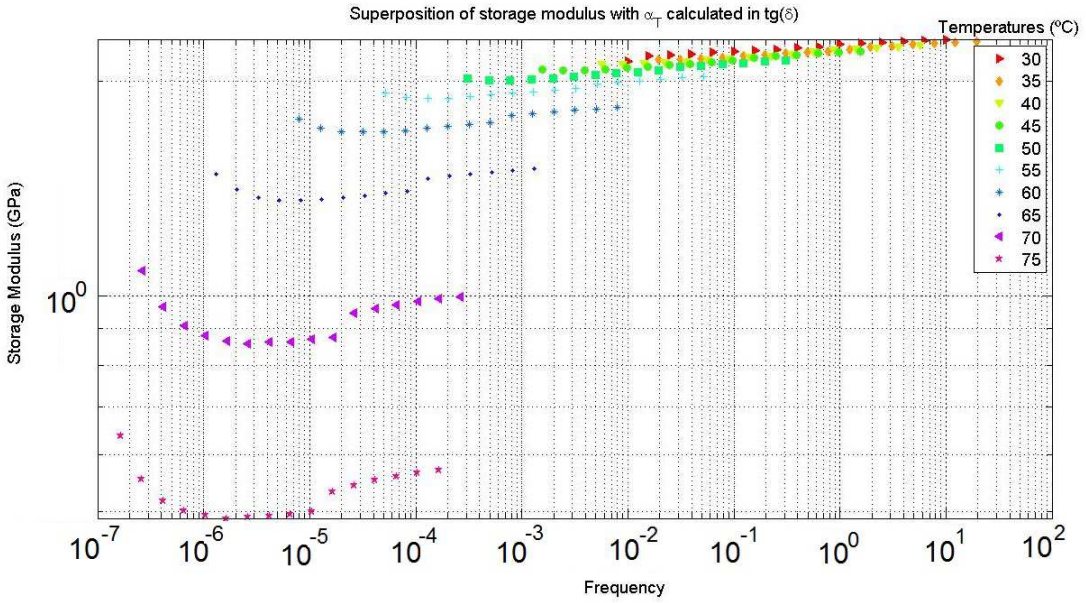

Figure 3.14: Storage modulus superposition for 200 μm ABS microparts with vertical shifting

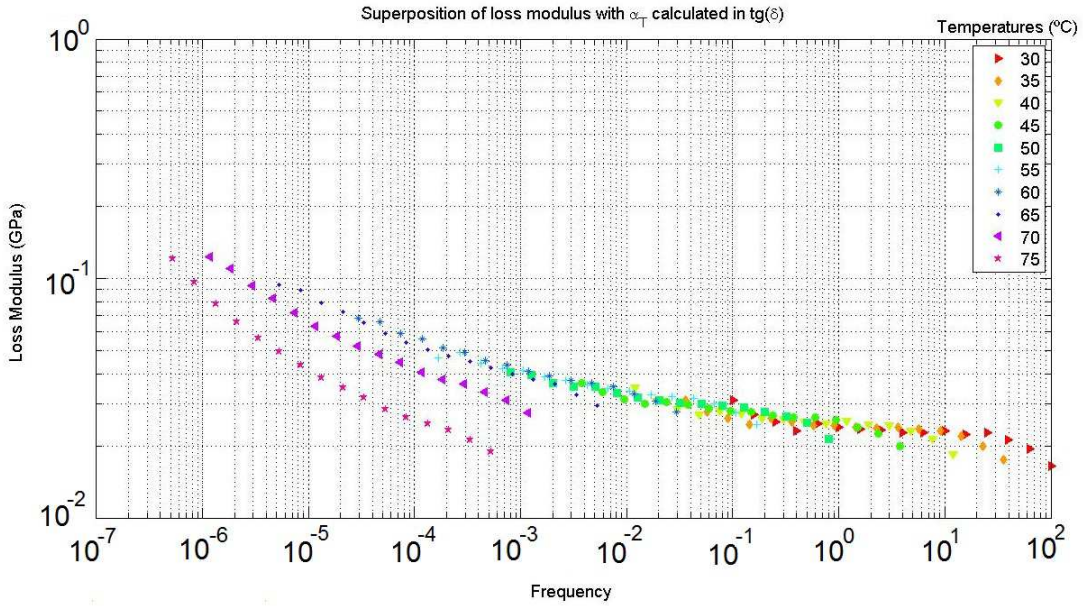

Figure 3.15: Loss modulus superposition for 300 μm ABS microparts with vertical shifting

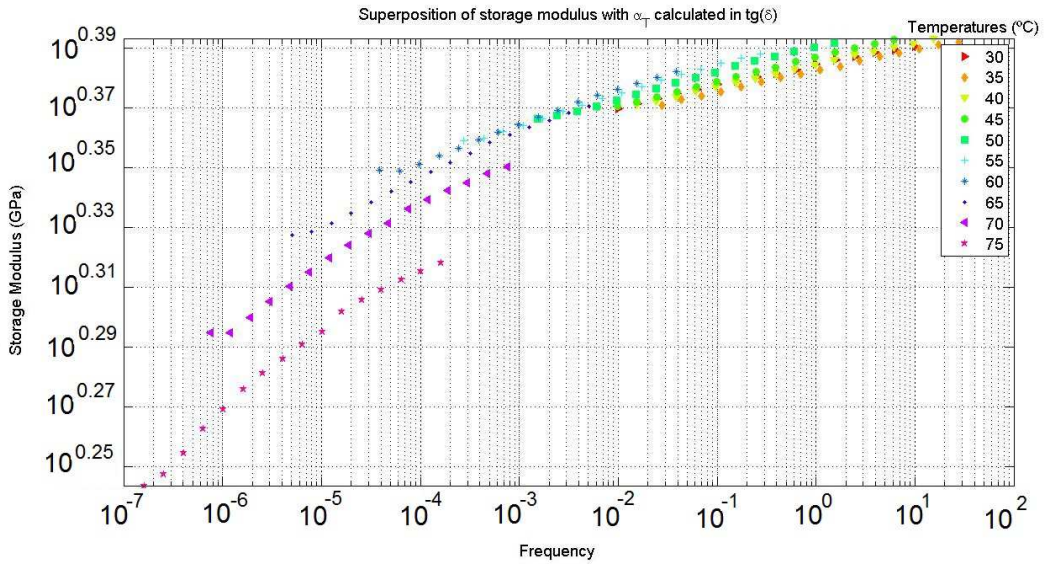

Figure 3.16: Storage modulus superposition for 300 μm ABS microparts with vertical shifting

At the end of the experiments, significant bending was observed in testing specimens. This is concomitant with numerical simulations in which similar boundary conditions were applied. Figure 3.17 shows the same bending mode in the test specimen and in the numerical simulation. This seems to be due to the fact that the DMTA machine clamps hold the micropart in the thicker area (400 μm) and the zone that suffers the most with the mechanical solicitation is situated after a change in the cross section (200 or 300 μm). This change in cross section tends to induce tensions that force the part to bend. This effect may be interfering with the measurement of the polymer properties and may bring some uncertainties to the measured properties.

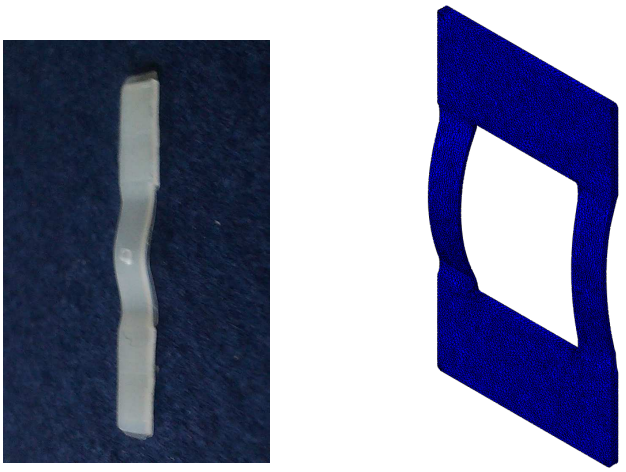

(a) Micropart after testing

(b) Tension numerical simulation with 1.59 scale factor

Figure 3.17: Micropart geometry influence on tests

600 μm micropart

A literature analysis revealed that TTSP should be able to be applied to ABS [14]. Therefore and in an attempt to cancel the bending effect that induced uncertainties, new test specimens with different geometry and thickness were produced via micro injection moulding , taking into account the same parameters as the previous microparts, as it can be seen in figure 3.18a. After injecting the new microparts in an Inautom D65 injection machine, samples were cut with an average size of $20 * 5 * 0.6$ mm, as it can be seen in figure 3.18b.

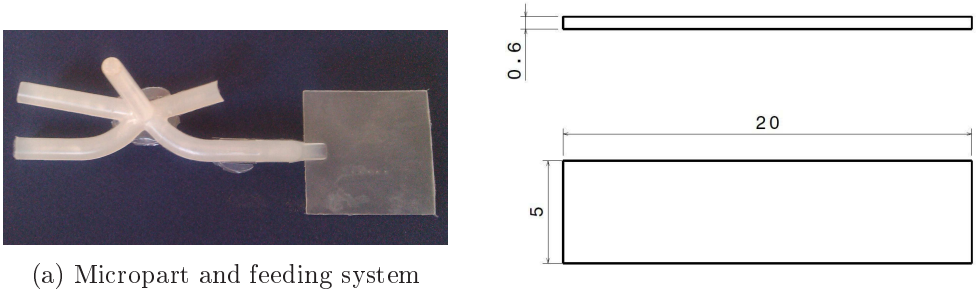

(a) Micropart and feeding system

(b) Micropart dimensions

Figure 3.18: Second micropart

The analysis for this micropart was done according to the same methodology previously referred.

For this new set of data, the Cole-Cole analysis suggests that the vertical shift factor is not necessary, i.e., material's properties show the same tendency, not changing with temperature. This absence of vertical shift can be noted in figure 3.19 since a superposition of curves occurs naturally, resulting in a single curve.

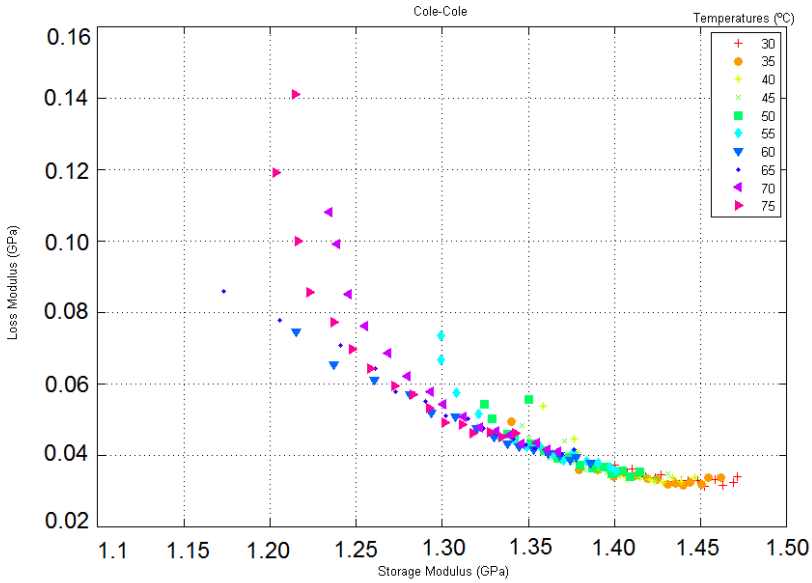

Figure 3.19: Cole-Cole plot for 600 μm ABS microparts

Figure 3.20 shows that the effect of b_T on the magnitude of the complex modulus is negligible and that data superimposes without shifting, composing a single curve (with some deviations from the tendency at higher temperatures) [7]. This suggests that the material is thermorheologically simple and that TTSP should now hold.

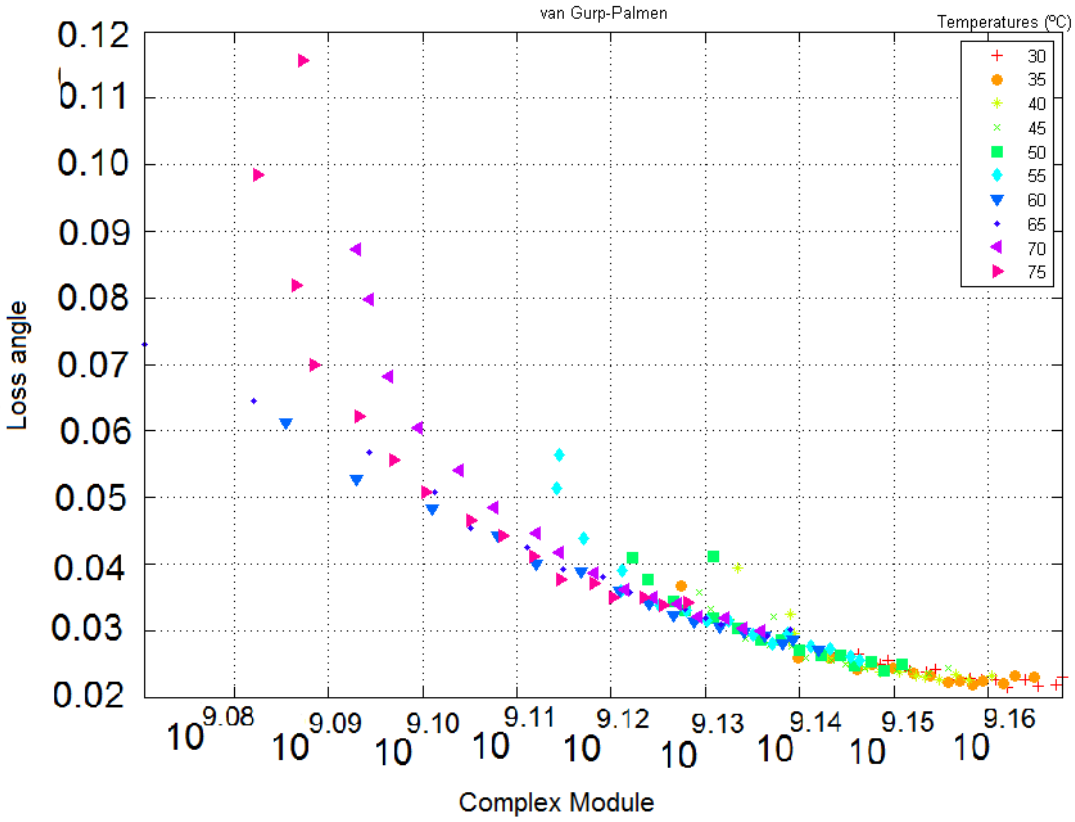

Figure 3.20: van Gurp Palmen plot for 600 μm ABS microparts

As the previous analysis indicated that the effect of vertical shift could be neglected, superposition was carried without reducing modulus.

Since the loss factor is a ratio of loss to storage modulus it is unaffected by vertical shifting. This way, it is possible to determine the horizontal shift factor without making any assumption about b_T [11][7].

Data obtained from DMTA for the loss factor can be depicted from figure 3.21.

Time temperature superposition principle was applied to the measured modulus and frequency, and reduced to a reference temperature of $30°C$. To achieve superposition, two methods were applied, both of them start from the same stage, the conception of an overlapping window as figure 3.22 shows.

The first method consists on discovering the mean value of the property that is being analysed. This mean value is calculated with the maximum and minimum value of the superposition window. After that, data are interpolated to obtain, for each curve, the frequency that originated the mean value. The process is resumed in figure 3.24.

This method requires few computational resources and revealed to be a good initial approximation to obtain shift factors. However, if the behaviour of the material is not

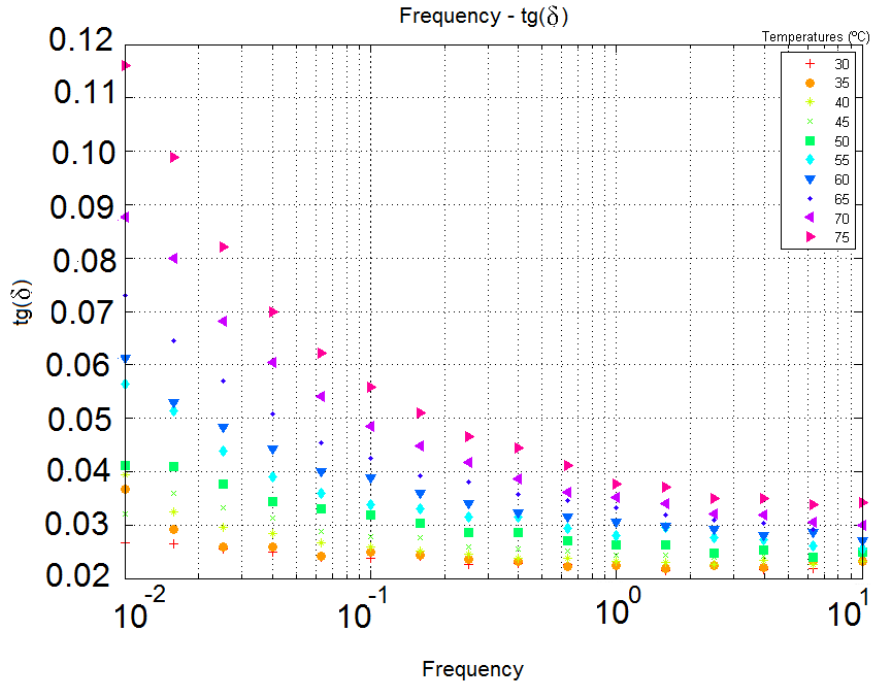

Figure 3.21: Loss factor experimental data for 600 μm ABS microparts

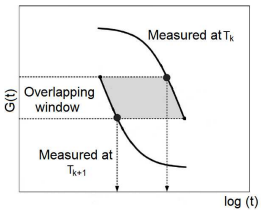

Figure 3.22: Overlapping windows for TTSP

constant through the middle section, interpolation errors may occur and the shift will be miscalculated. Also, data acquisition errors during the experiment may yield bad results for $\alpha_T(T)$. Hence this method was applied to data loss factor and the master curve presented in figure 3.24 was obtained.

A second method was created in an attempt to suppress the first method possible flaws. It is based on an iterative cycle where for each $'m'$ increment, the horizontal error is calculated when shifting adjacent curves. To achieve so, the horizontal distance between $'n'$ points for the same value in the vertical axis is calculated and divided by the horizontal axis value of the fixed curve, obtaining a relative error. Then the decision of which increment yields the best superposition is based on the minimum of the mean error for each iteration, calculated as the sum of the squared errors divided by the number of points. The process is represented in figure 3.25.

Applying this second method to the same data yields the master curve presented in figure 3.26.

A visual inspection reveals that a better superposition can be achieved with the second method, based on the fact that a smoother curve is obtained. The first method

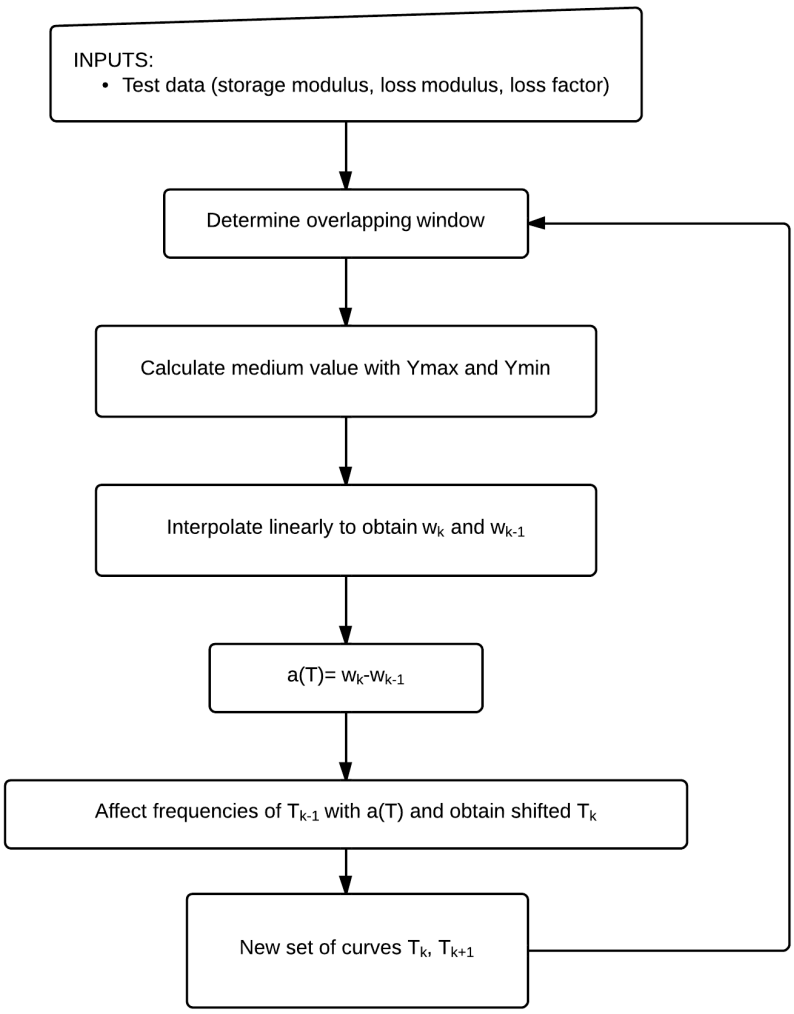

Figure 3.23: Flow chart for TTSP first method

yielded a master curve that failed in superposing the lower temperature curves, creating some gaps between them. Therefore different values for shift factors were obtained and can be found in table 3.2

These values should be interpreted as the ones that separate two adjacent curves. Therefore, when using them to further interpretations they should be added or subtracted progressively with the latter.

Master curves for storage and loss moduli were obtained as can be seen in figures 3.27 and 3.28, respectively.

The criterion that states that the same values of $\alpha_T(T)$ must superpose all the viscoelastic functions appears to be fulfilled [22][10] . However, it must be noted that some experimental points lie out of the master curve tendency. This can be due to some secondary transitions that may be occurring since the vitreous transition of ABS is around $93°C$. Since this behaviour can also be noticed at lower temperatures, both systematic and random errors should be considered, such as an incorrect mounting position of the

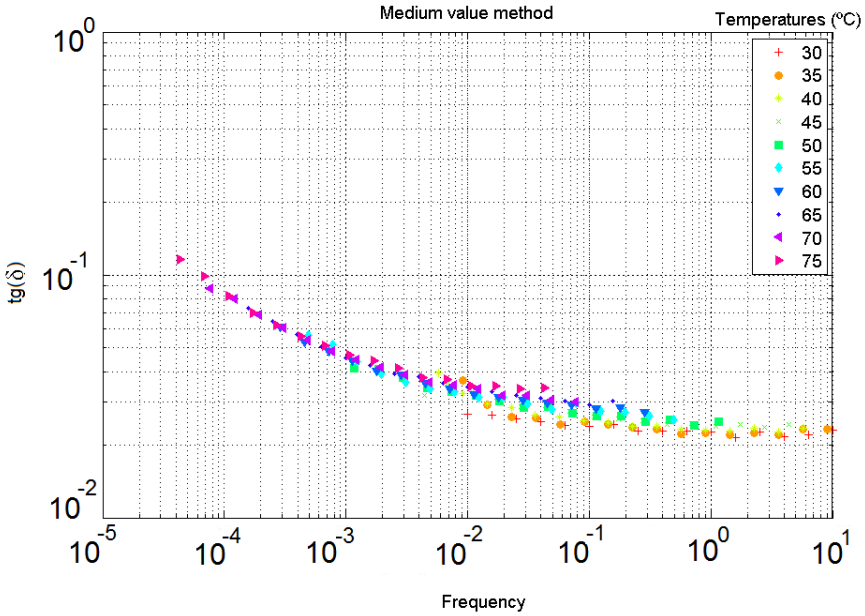

Figure 3.24: Master curve for loss factor with mean value method, Tref=30°C for 600 μm ABS microparts

Table 3.2: Log $\alpha_T(T)$ obtained through first and second methods

Temperatures(°C)	Log $\alpha_T(T)$ first method	Log $\alpha_T(T)$ second method
30-35	-0.0410	-0.1603
35-40	-0.2007	-0.5330
40-45	-0.1165	-0.7494
45-50	-0.5763	-0.4669
50-55	-0.3750	-0.7074
55-60	-0.2342	-0.2986
60-65	-0.2588	-0.5090
65-70	-0.3126	-0.2805
70-75	-0.2524	-0.4428

test specimen [19]. These shift factors may now serve as basis to calculate the constants present in equations such as the William Landel Ferry (WLF) or the Arrhenius one.

In order to calculate the activation energy for the Arrhenius, the following equation was used [12]

$$Log_{10}\alpha_t(T) = \frac{\Delta H}{2.303R}\left(\frac{1}{T+273.15} - \frac{1}{T_0+273.15}\right) \tag{3.1}$$

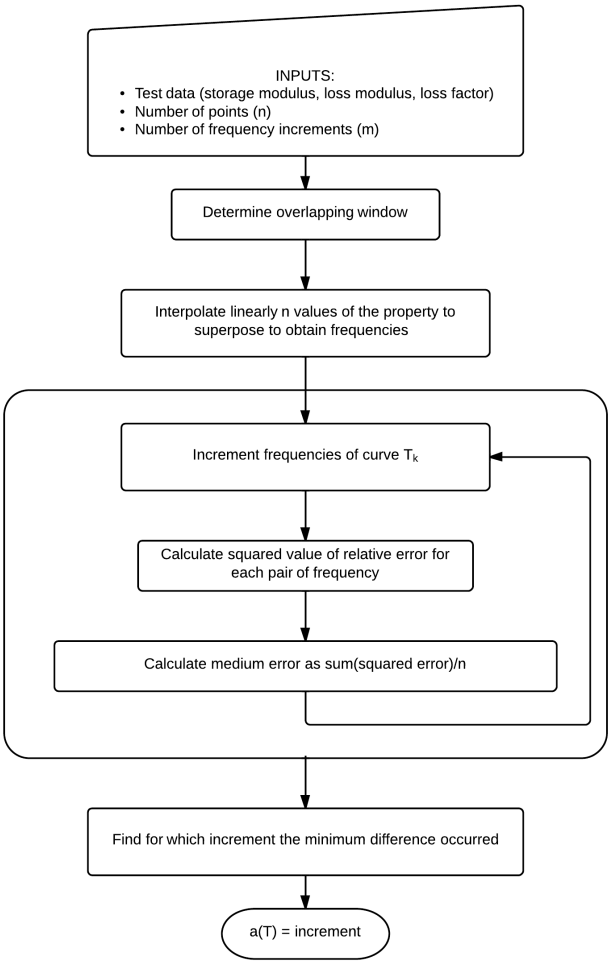

Figure 3.25: Flow chart for TTSP second method

where ΔH is the activation energy of the relaxation process and $R = 1.98 * 10^{-3}$ kcal/mol. Through the equation 3.2 linearization, the activation energy ΔH can be obtained as a function of the slope of $Log_{10}\alpha_t(T)$ versus $(1/T) - (1/T_0)$. Figure 3.29 shows the linear regression of the data.

The temperature dependence of the horizontal shift factor follows an Arrhenius equation ($r^2 = 0.991$) and the activation energy revealed to be 198,4 kJ/mol.

For the WLF equation the methodology used was the one presented in [10]. Starting from the WLF equation it is possible to get:

$$\frac{T - T_0}{log_{10}\alpha_t(T)} = -\frac{1}{c1}(T - T_0) - \frac{c2}{c1} \tag{3.2}$$

This way it is possible obtain c1 and c2 from a linear regression of $(T - T_0)/log\alpha_T$ versus $T - T_0$, where if s represents the slope and i the intersection, c1 and c2 can be obtained as:

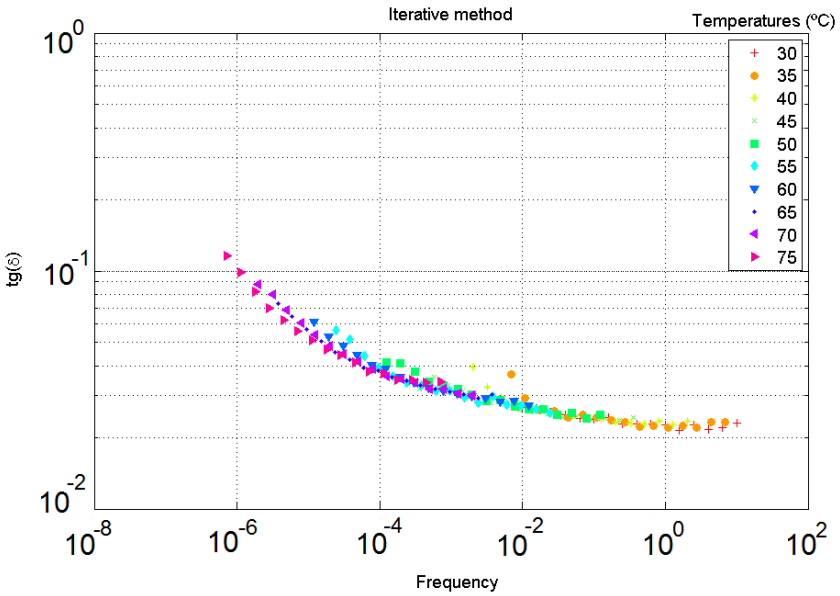

Figure 3.26: Master curve for loss factor with iterative method, Tref=30°C for 600 μm ABS microparts

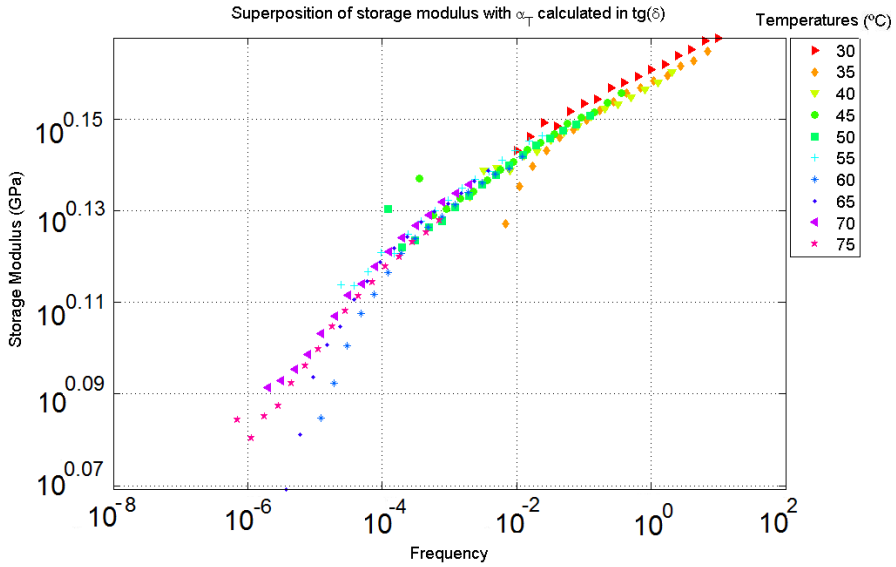

Figure 3.27: Master curve for storage modulus for 600 μm ABS microparts

$$c_1 = -\frac{1}{s} \tag{3.3}$$

$$c_2 = \frac{i}{s} \tag{3.4}$$

Applying this formulation to obtained data results in c1=52.4456 and c2=513.771. Another approach to calculate values for c1 and c2 can be found in the literature [13].

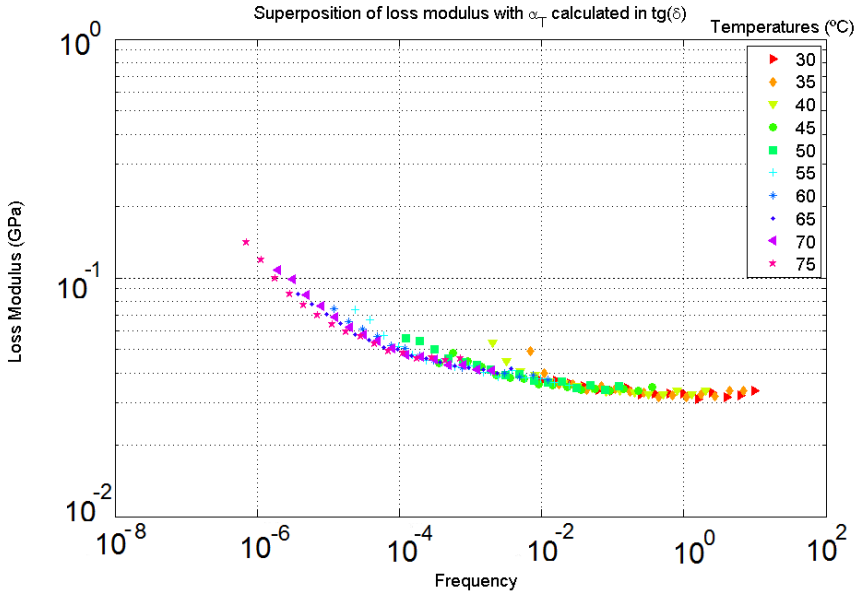

Figure 3.28: Master curve for loss modulus for 600 μm ABS microparts

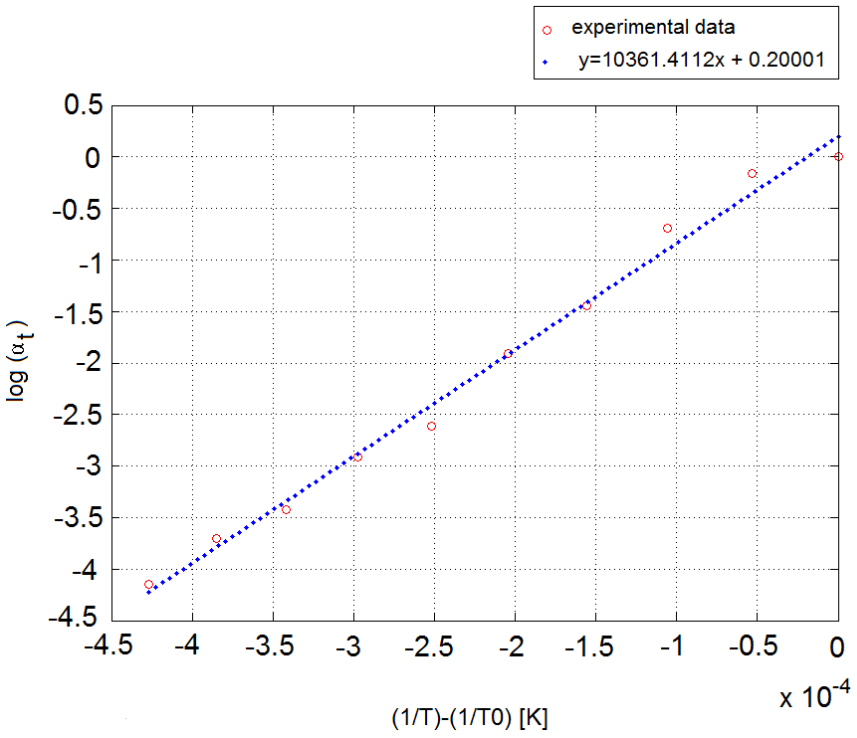

Figure 3.29: Linear regression for activation energy

Despite some slight deviations, it can be seen that the horizontal shift factors obtained by the second Matlab® algorithm comply with either WLF or Arrhenius equation. A graphical comparison can be seen in figure 3.30.

It can then be concluded that ABS behaves as a thermorehologically simple polymer

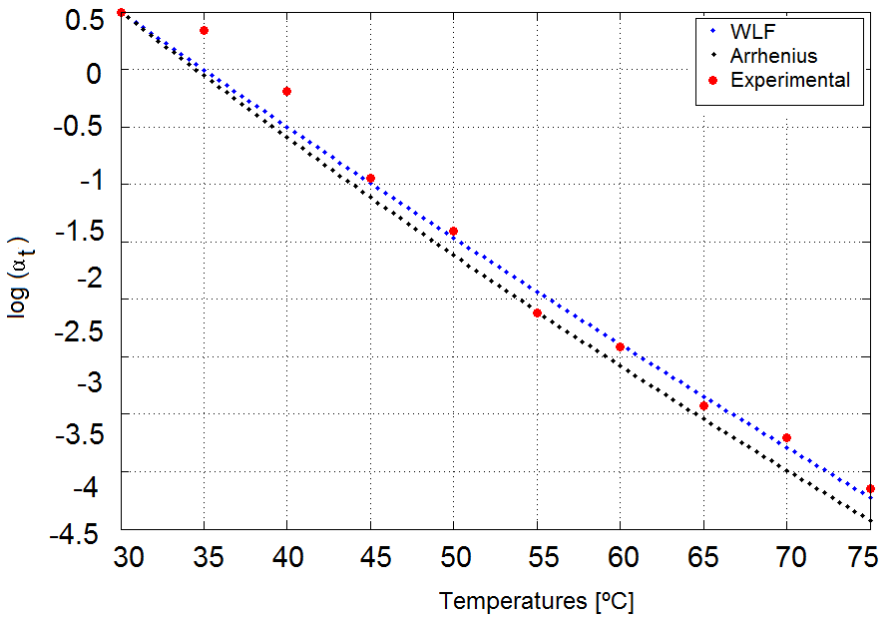

Figure 3.30: Comparison of Arrhenius and WLF equations curve fitting with experimental data for ABS at several temperatures

and therefore it can be subjected to TTSP. Two simple algorithms were implemented and one of them validated with basis on the empirical equations for calculating shift values. Deviations at higher temperatures were noticed and can be due to secondary transitions or due to the fact that the temperature is approaching the vitreous transition zone since ABS is an amorphous polymer. As it was mentioned before, some experimental errors associated with deficient experimental set-up may not be disregarded to have influenced the results.

Chapter 4

Polymer micropart - numerical analysis

Injection moulding is a very common technique to produce commonly used parts and a major consumer of all plastics. This large extent in use of plastics constitutes a necessity to improve processing techniques in order to make production more efficient. Each plastic differs from the other, having its own properties that make it suitable for different applications. Therefore each of them requires different processing and injection moulding procedures and parameters [20]. These parameters may have significant importance in the performance of the part when in duty.

In fact, after injection and packing, the molten plastic starts to shrink and internal stresses start developing. Residual stresses are process-induced stresses and are related to the referred injection parameters. They can be either flow induced, generated by viscoelastic deformations or thermally induced due to the temperature gradients that start to develop.

Zhil'tsova *et al.* [25], studied the influence of residual stresses in moulded parts with metallic inserts. Here, residual stresses tend to be larger, since metals have a thermal expansion coefficient much smaller $(10 - 20 \cdot (10^{-}6)^{\circ}C^{-1})$ than polymers $(100 - 200 \cdot (10^{-}6)C^{-1})$, not allowing for polymer's contraction. When a part is ejected, geometrical constraints are removed and part's dimensions suffer major changes due to the stresses accommodation process that starts to develop. Beyond plastic properties and process parameters, part design also may influence the development of residual stresses. However the injection temperature appears to be one of the most critical variables since a drop in temperature at the flow front affects negatively the bonding of molecules, weakening the final product [25].

This chapter aims to establish a methodology allowing to evaluate the influence of process induced stresses in a part performance during its lifetime.

Process induced stresses can be obtained through injection simulation. In fact, when a Moldflow® fill-pack-warp analysis is performed, residual stresses after cooling in the mould may be obtained as an output. Moldflow® has a specific tool named AMI Abaqus® interface to convert data from the analysis so it can be post-processed. Running this macro yields as output the following files:

- mechanical properties;

- partial input file for Abaqus®,
- residual stresses file.

The last two files are of major importance. The first contains nodal coordinates, element topology, element properties and boundary conditions sufficient to eliminate the structure's rigid body modes. The second contains residual stresses description in principal directions (no shear values) associated with that mesh in particular. Commonly the program uses 4-node tetrahedral (C3D4) elements.

In order to obtain the residual stresses, Moldflow® micro-parts simulations were obtained by courtesy of the work group in which this dissertation is inserted into. These simulations served as basis to predict the process settings according to which micro parts would be processed. Figures 4.1a and 4.1b show the complete injection system and the micro-part with an optimized mesh.

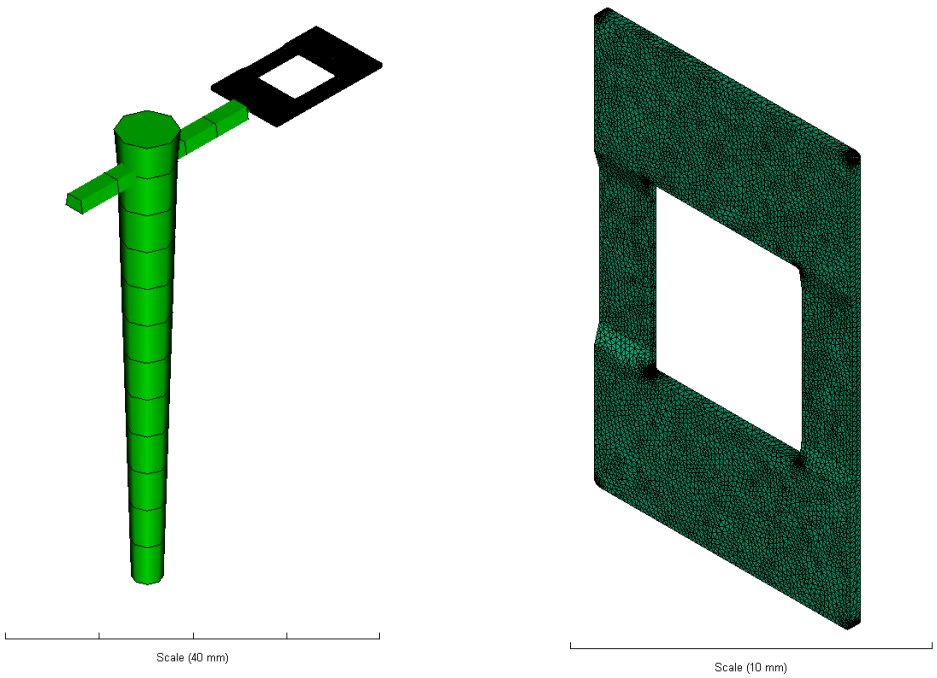

(a) Injection system and part

(b) Micro part in detail

Figure 4.1: Micropart in analysis

After running the macro for the presented parts, the referred partial input file was obtained. This partial input file may be readily submitted for analysis in order to visualize the residual stresses but for further analysis it needs to be largely modified. To do so the following statement should be used in a command line: $abaqus\ job = 'file'.inp\ interactive$.

Moldflow® yields a "*.ist*" where the residual stress are given as 'Element' 'S11 S22 S33 S12 S13 S21'. One line of this file can be seen in figure 4.2, where the initial state of stress of the part is represented and the stress value read in Abaqus® for the same element is also shown.

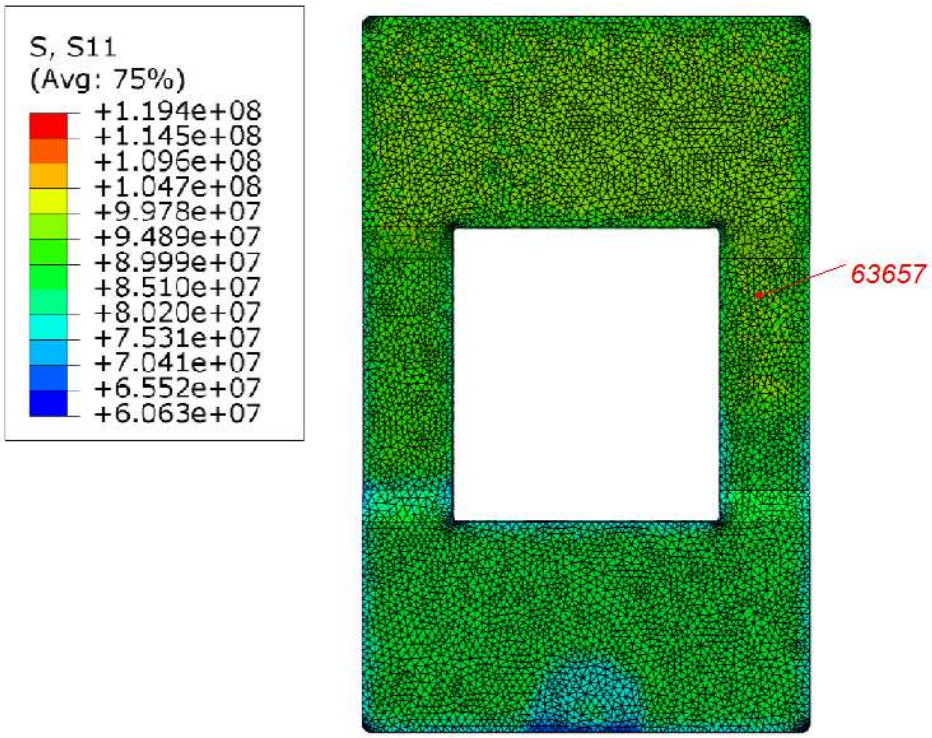


```
Element: PART-1-1.63657
  Type: C3D4
  Material: ABS
  Section: EALL.Section-ASSEMBLY_PART-1-1_EALL, Homogeneous Solid Section, Thickness = 1
  Connect: 87994, 80018, 87960, 110992
  S, S11 (Not averaged): 9.26343e+07

63657,    9.26343e+007,    9.26343e+007,    9.26343e+007,    0.00000e+000,    0.00000e+000,    0.00000e+000
```

Figure 4.2: Initial state of stress, reading from file

Once residual stresses are defined in terms of principal directions, shear stresses become null. Also these stress values are equal in the three principal directions. Therefore von Mises equivalent stresses assume a zero magnitude at the start of the analysis.

Since residual stresses are obtained in the moment that the mould constraints are removed, and because different shrinkage occurs, the field of stresses is not uniform as the color map in figure 4.2 suggests. Therefore a process of internal stresses stabilization occurs which leads to part volume modification and possible warpage.

When simulating this behaviour computationally, it is then necessary to include one stabilization step, in which boundary conditions that restrict rigid body modes are used to prevent part from accelerating and moving freely. Also this allows to see part's distortion. Figure 4.3 shows, with an amplification factor of 50, the shrinkage and deformation that the part suffers due to the non uniform distribution of initial stresses.

It can be noted that the larger warpage is in the top of the micro part, opposed to the gate position. This is due to the fact that when the part is almost completely filled it starts to cool being the gate zone where the larger portion of molten polymer is found,

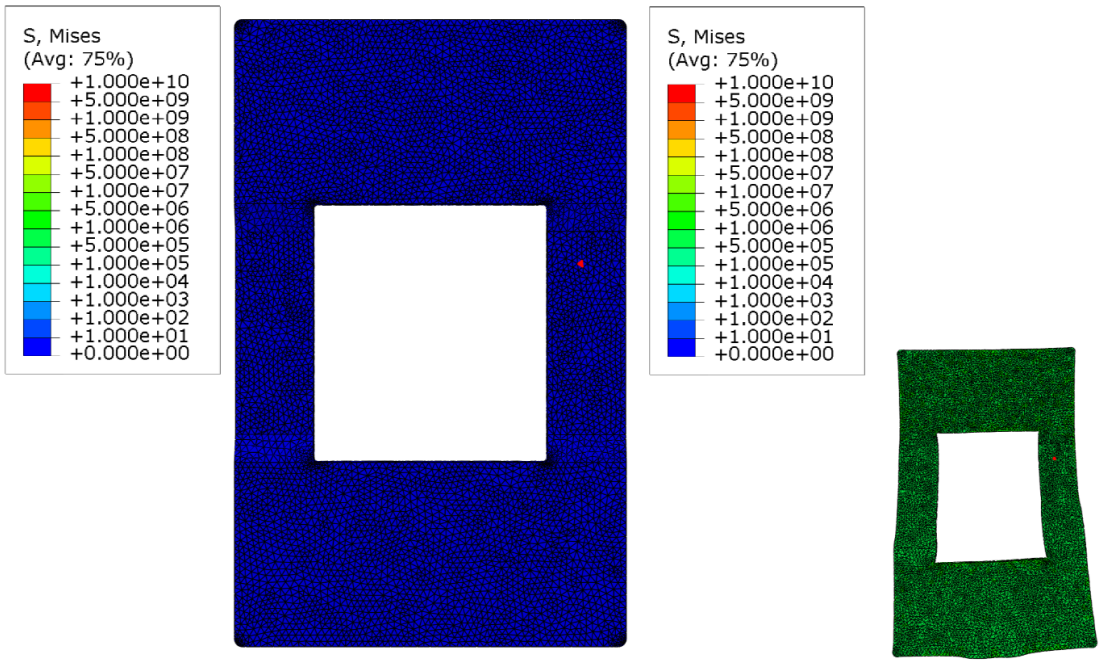

Figure 4.3: Part deformation and shrinkage, scale factor of 50

constituting a hot spot that slows polymer shrinkage. This way molecules in polymer have more time and space to accomodate themselves, yielding lower residual stresses.

Once the initial stress state of the micro-part post-processing is obtained, it is of interest to study their influence on the part behaviour when subjected to mechanical stress during its lifetime. Therefore, the analysis follows as a relaxation test where a viscoelastic model is necessary to simulate the polymer's behaviour. To achieve this a second static step was created, where a strain of 20 μm is imposed to one end of the part whilst the other is fixed.

Figure 4.4a shows the stress field for the $300\mu m$ zone of the micropart (future analyses will be done with this area as an example), after being stretched. It can be immediately seen from the dominant colors that stresses increase as the zone in the analysis approaches the middle of the part, as it would be expected. Figure 4.4a also shows three different elements within the zone to be further analysed.

The color map from figure 4.4a shows a predominant yellow color which suggests that higher levels of stress are present comparatively to figure 4.4b. Since the same color map was selected in both figures a more profound analysis on the value of the von Mises equivalent stress for the depicted elements reveals that the presence of residual stresses has a massive impact on stress levels. Table 4.1 presents the von Mises equivalent stresses for the three different elements through the length of the part and the percentual increase due to the residual stresses.

The percentual values reveal that the increase in stress is unexpectedly high. This may be due to several reasons. One of them is the fact that the elastic modulus obtained in DMTA tests for the higher frequency at the lower temperature (where the loss component of viscoelasticity is diminished since molecules do not have time to adopt minimum energy positions) revealed to be lower than the value indicated by the polymer manufacturer,

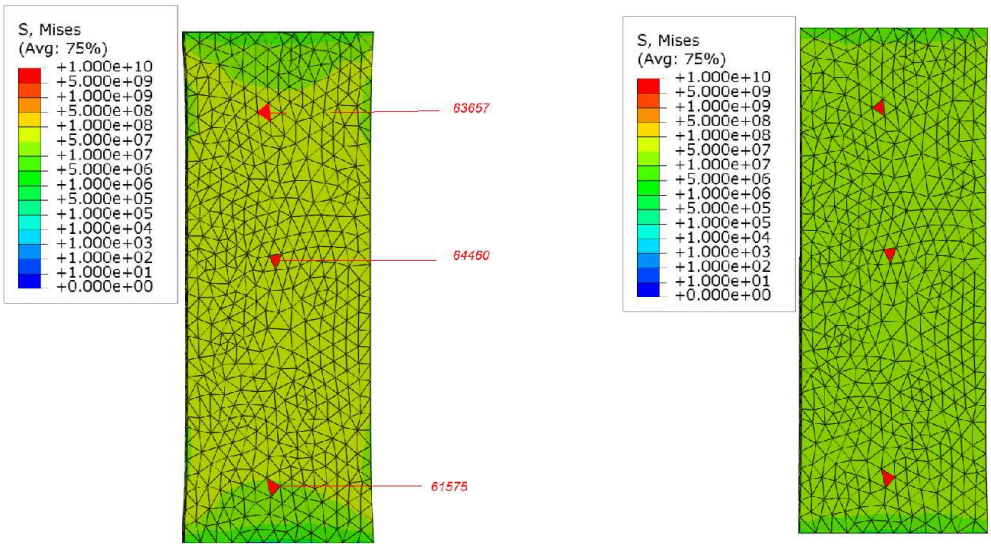

(a) With initial stresses

(b) Without initial stresses

Figure 4.4: Field of stresses when a $20\mu m$ strain is imposed (true deformation scale factor)

Table 4.1: Influence of initial stresses on the stressed zone

Element	With residual stresses $[Pa]$	Without residual stresses $[Pa]$	Percentual increase [%]
63657	$3.05099 \cdot 10^7$	$8.62303 \cdot 10^6$	253.8
60460	$3.26425 \cdot 10^7$	$8.81743 \cdot 10^6$	270.2
61575	$2.33771 \cdot 10^7$	$8.03875 \cdot 10^6$	190.8

$2.4GPa$. This value can be either obtained in polymer's data-sheet or in Moldflow® database and may influence the calculation of residual stresses, yielding higher values than expected. Also, according to Boltzmann superposition principle, stress responses to successive deformations are additive and therefore, these initial stresses will increase the total value of stress as figures 4.6, 4.7 and 4.8 show. Another reason which can explain the discrepancy between values is the fact that after cooling and being ejected from the mould, micro-parts tend to shrink further. When applying the same displacement to a shrunken part and to a part without initial stress the strain rates will be different and therefore different values of stress will be obtained since the same displacement will induce a larger strain value.

To proceed simulating the relaxation test, viscoelasticity must be taken into account. Abaqus® allows multiple ways of inserting viscoelastic data such as creep test data, relaxation test data, frequency-dependent test data or even direct specification of Prony series parameters ($\bar{g}_i^P$, $\bar{k}_i^P$ and τ_i). The latter was chosen since DMTA test results are frequency dependent.

Frequency domain data are defined in a tabular form, by providing as input the

real and imaginary parts of $\omega g*$ as function of frequency in cycles per time. If $G_s(\omega)$ designates the storage modulus and $G_l(\omega)$ the loss modulus, the real and imaginary parts can be obtained as [5]

$$\omega\Re(g^*) = \frac{G_l}{G_\infty} \tag{4.1}$$

$$\omega\Im(g^*) = 1 - \frac{G_s}{G_\infty} \tag{4.2}$$

Here, G_∞ is the long-term modulus, obtained from elastic properties (when $t \rightarrow \infty$).G_∞ is obtained as the storage modulus value for which the minimum frequency occurs. Since frequency is the reciprocal value of time this is the same as obtaining the modulus for the longest value of time possible.

The Matlab® developed application calculates automatically the parameters of viscoelastic model. These values are calculated having the master curves previously generated as base data. The program generated values are shown in table 4.2.

Table 4.2: Real and Imaginary part values for calibrating viscoelastic model

G* Real	G* Imaginary	Frequency [Hz]
0.119521	-0.05694	3.39E-6
0.10016	-0.252621	1.26E-005
0.0703479	-0.262141	4.23E-005
0.0584746	-0.287159	0.000101767
0.0464621	-0.346769	0.00101763
0.0428491	-0.372563	0.00214426
0.0385594	-0.399576	0.0142132
0.0350469	-0.41453	0.0364421
0.0338099	-0.42357	0.245169
0.0341313	-0.47817	10

These values can now be used to calibrate the Prony series terms. Abaqus® uses analytical expressions to relate the Prony series relaxation functions to the storage and loss moduli. Figures 4.5a and 4.5b show the calibrated model created by Abaqus® and its comparison with experimental tests data.

A better agreement can be found between the loss component of the model produced by Prony series calibration and test data for the loss modulus. As seen before, a better superposition was obtained for the loss modulus relatively to the one obtained for the storage modulus. Even though figure 4.5a shows deviations from test data, the maximum RMS error committed is small, 1.7%.

In order to simulate the relaxation process another step is required. Therefore, a third "$*Visco$" step was added to the "*.inp*" file, maintaining the previous defined boundary conditions. Figures 4.6, 4.7 and 4.8 show the evolution of stress levels during the whole analysis. Two figures per element are shown since the initial state of stress and the displacement are imposed in much smaller intervals of time than the relaxation process takes to occur.

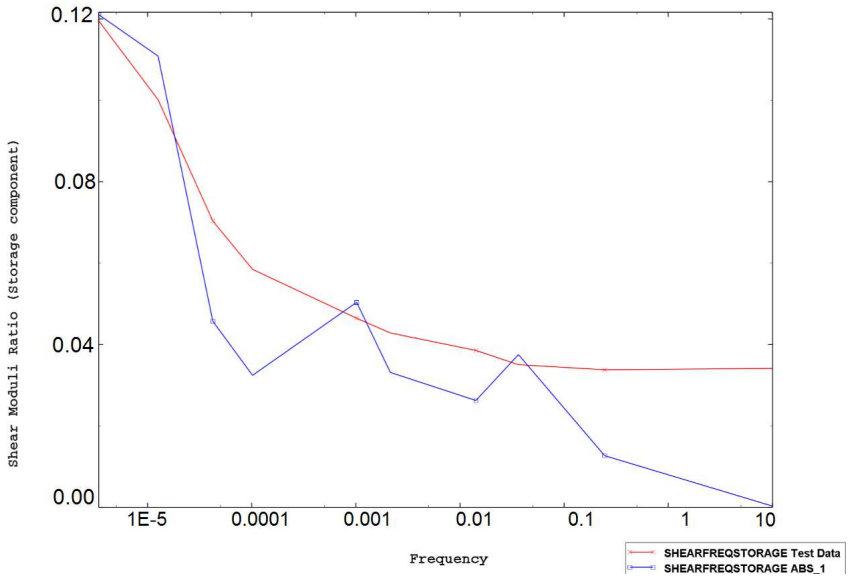

(a) Test data vs computed data for storage component

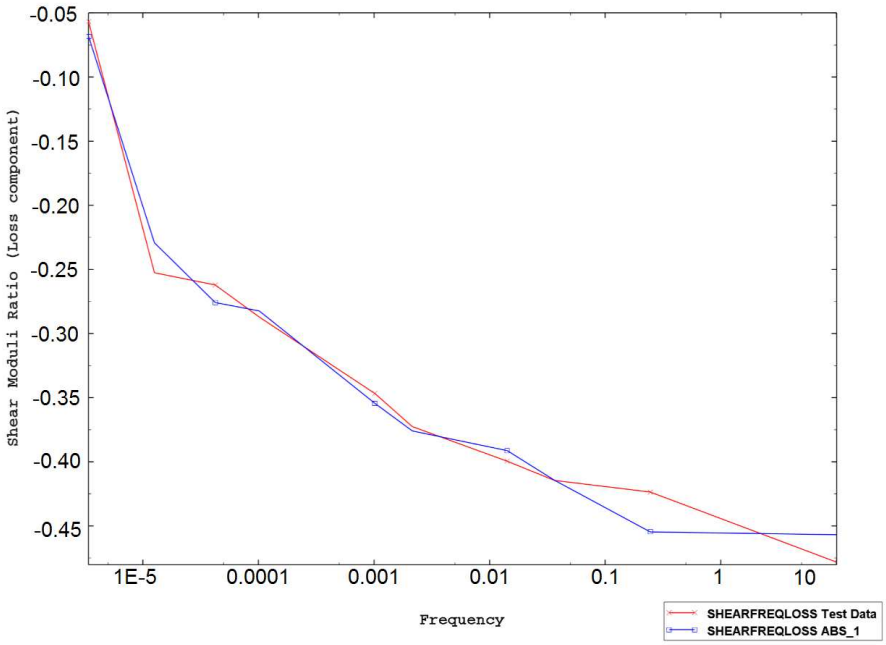

(b) Test data vs computed data loss component

Figure 4.5: Viscoelastic model calibration

It is possible to note that blue curves suffer linear increments of stress between 0-2s. The first increment is related to the presence of initial stresses. Despite the fact that figure 4.2 shows that initial stresses exist at $t = 0s$ it must be noted that the present analysis is based on von Mises equivalent stresses and therefore, the starting value in these figures is zero. At the end of the first step, $t = 1s$, an equilibrium state is reached and the value of stresses increased due to the initial stresses. At this point green curves show no

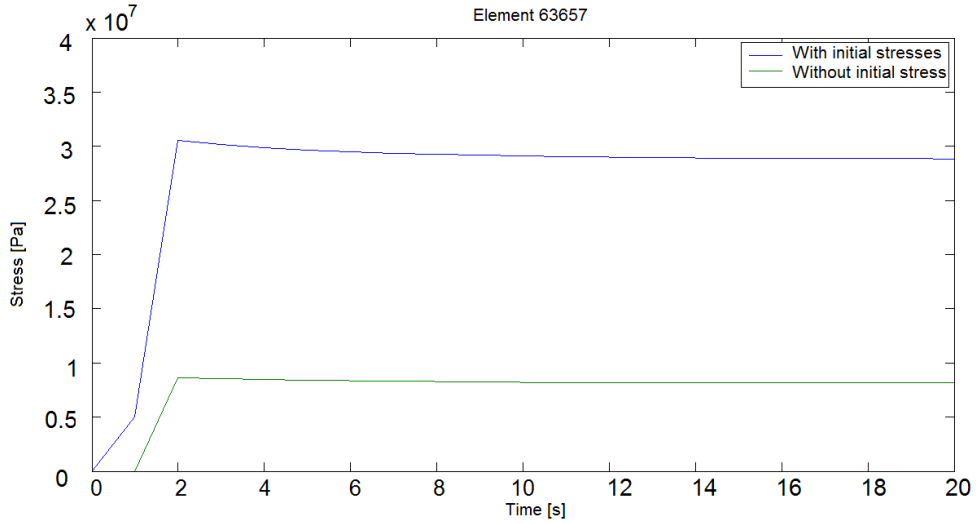

(a) Reduced time scale

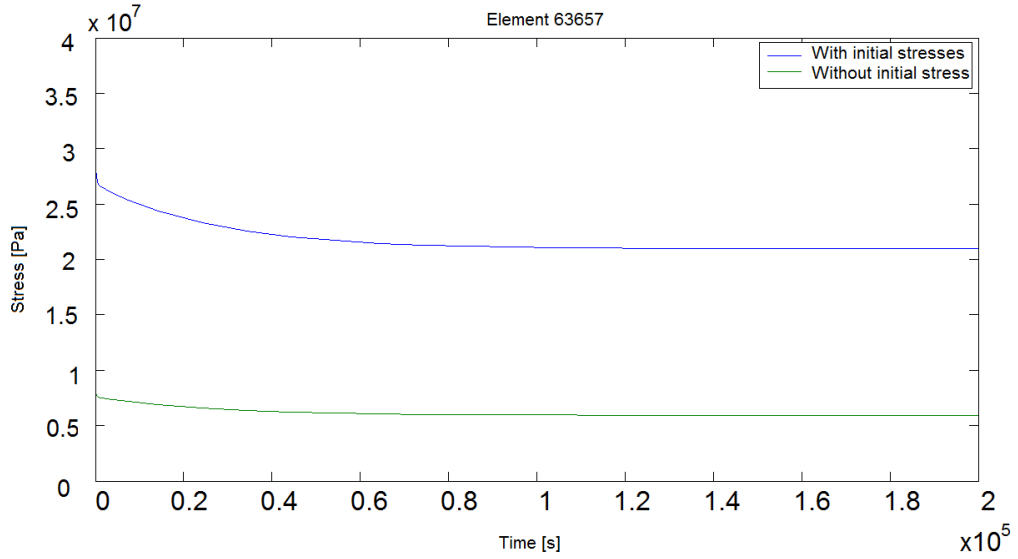

(b) Full time scale

Figure 4.6: Element 63657 stress evolution

stress values since they are absent. The second stress increment, from $t = 1s$ to $t = 2s$ is due to the imposed strain. A more detailed analysis on the stress levels generated in this step reveals that the yield stress of the polymer, 45 MPa, is not exceeded. From $t = 2s$ on, curves show a gradual decrease in stress caused by the definition of the material as viscoelastic. Here, the program starts to take into account the loss component of the material. This results in the gradual reduction of the stress levels similarly to what happens in a real relaxation test, in which molecules tend to arrange themselves in a minimum energy state and to accommodate stresses. Tables 4.3 and 4.4 present stress levels for $t = 2s$ and for $t = 200000s$, corresponding to the moment when the viscoelastic model is implemented and the end of the numerical simulation.

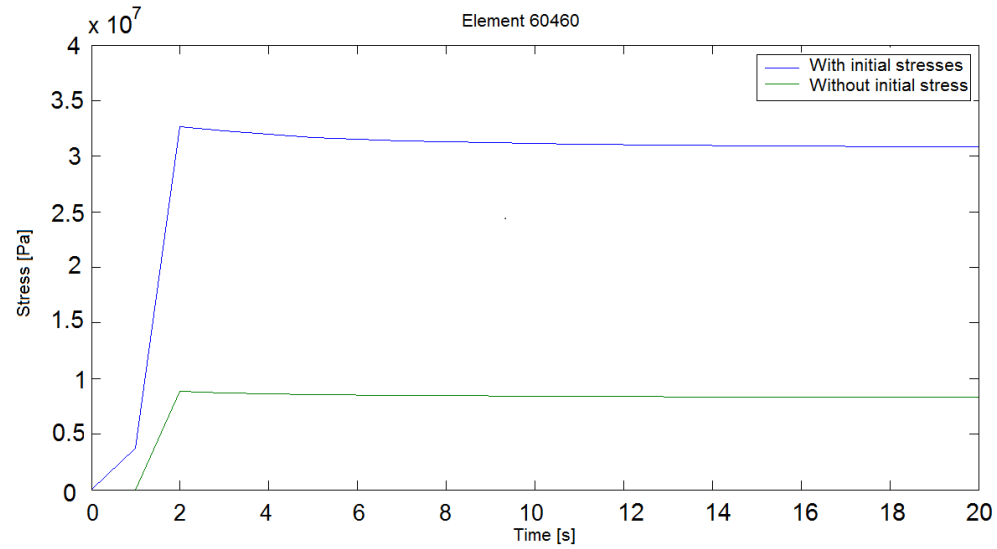

(a) Reduced time scale

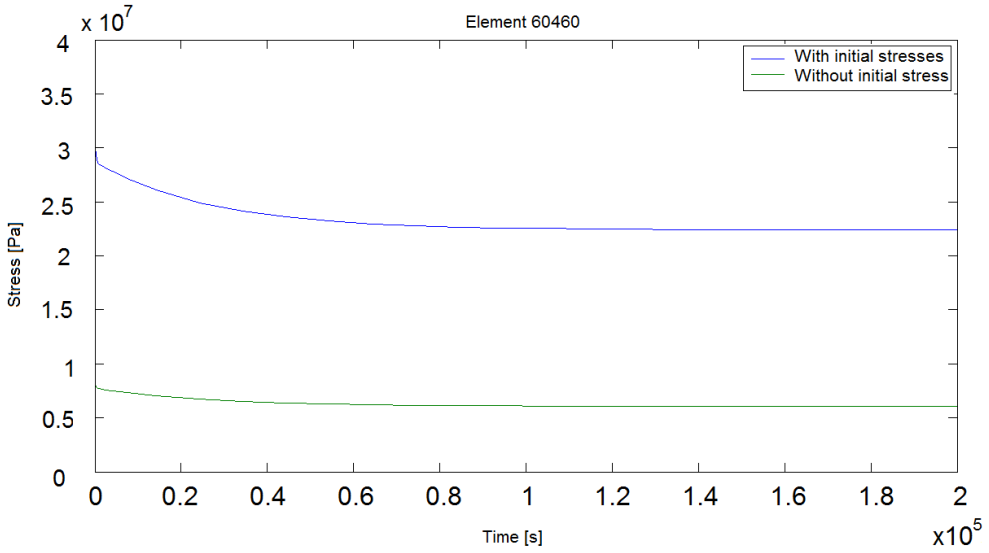

(b) Full time scale

Figure 4.7: Element 60460 stress evolution

Here it is possible to observe that, despite the influence of initial stresses on stress magnitudes, the relaxation process is not affected by the stresses magnitude for these low strain levels. In fact, a percentage decrease of 31% was obtained for the three elements in study.

In order to evaluate limits of linear viscoelasticity, a strain of 1% was imposed. Figures 4.9 and 4.10 show stress values for the majority of the elements that compose the interest zone in analysis.

A closer inspection of the stress levels depicted in figure 4.9 reveal that the yield tensile stress of the polymer is still not surpassed. However, when initial stresses are

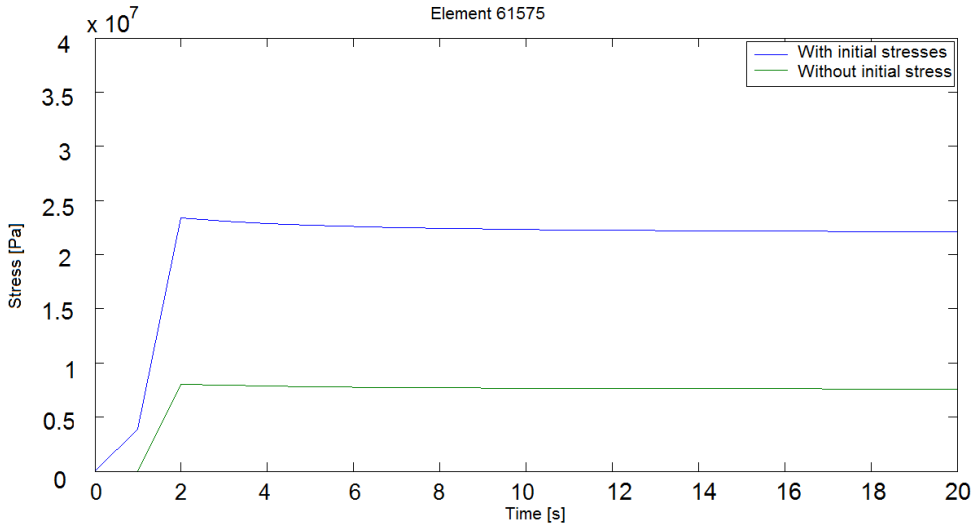

(a) Reduced time scale

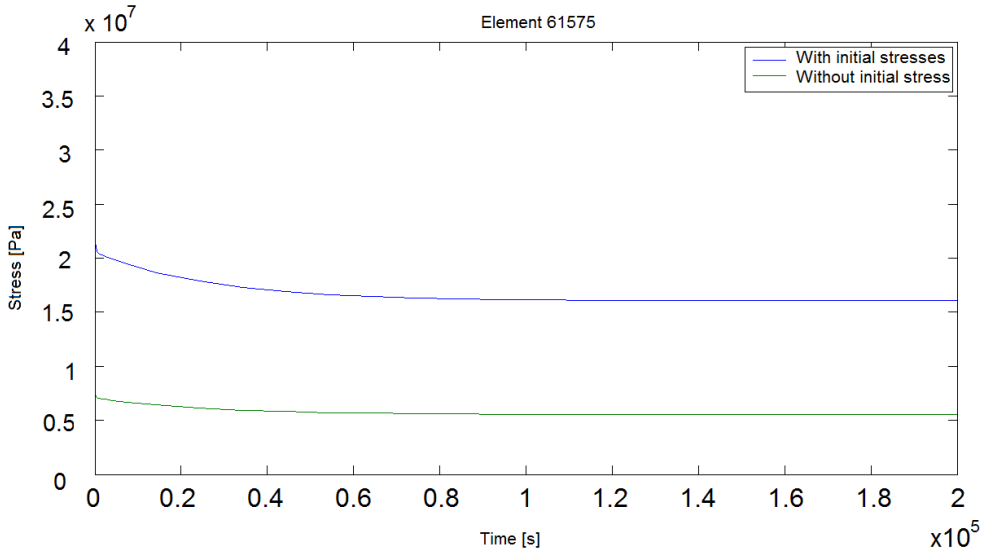

(b) Full time scale

Figure 4.8: Element 61575 stress evolution

Table 4.3: Viscoelastic model influence on stress decrease, with initial stresses

Element	Stress before relaxation $[Pa]$	Stress after relaxation $[Pa]$	Percentual decrease [%]
63657	$3.05099 \cdot 10^7$	$2.09454 \cdot 10^7$	31.3
60460	$3.26425 \cdot 10^7$	$2.24095 \cdot 10^7$	31.3
61575	$2.33771 \cdot 10^7$	$1.60487 \cdot 10^7$	31.3

Table 4.4: Viscoelastic model influence on stress decrease, without initial stresses

Element	Stress before relaxation $[Pa]$	Stress after relaxation $[Pa]$	Percentual decrease [%]
63657	$8.62303 \cdot 10^6$	$5.91981 \cdot 10^6$	31.3
60460	$8.81743 \cdot 10^6$	$6.05327 \cdot 10^6$	31.3
61575	$8.03875 \cdot 10^6$	$5.5187 \cdot 10^6$	31.3

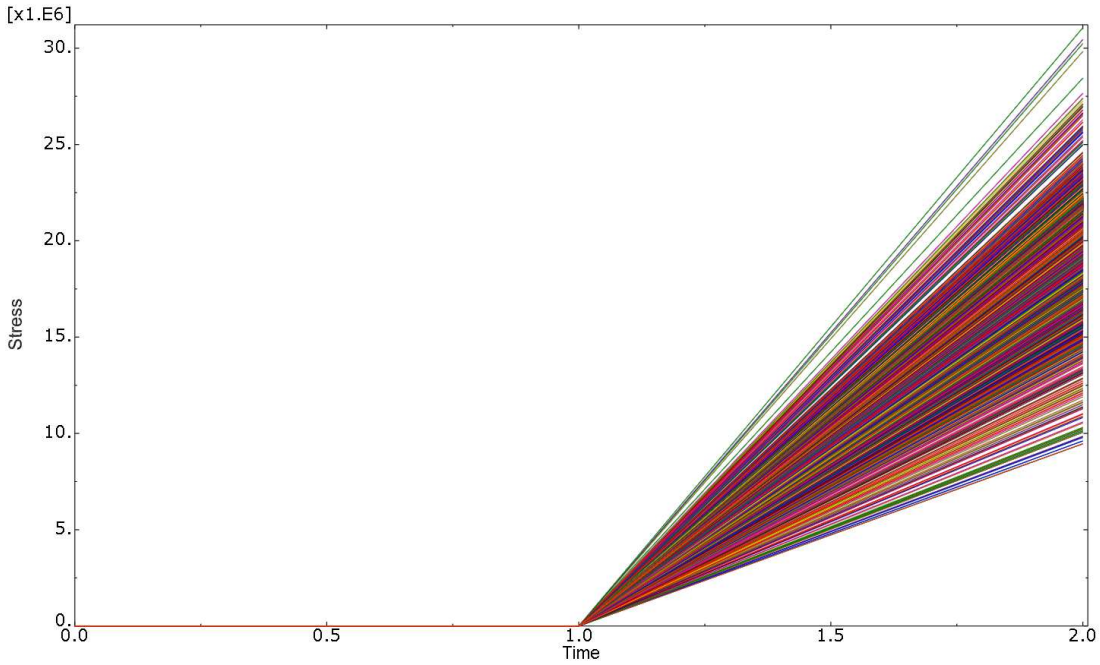

Figure 4.9: 1% strain without initial stresses

taken into account, stress levels in several elements may exceed polymer's yield tensile stress, as can be seen in Figure 4.10. This indicates that the part may not be in a state of elasticity and might deform plastically.

Therefore, the viscoelastic limit of 1% may not be assumed as correct for parts obtained via micro injection moulding. However, this subject needs further investigation.

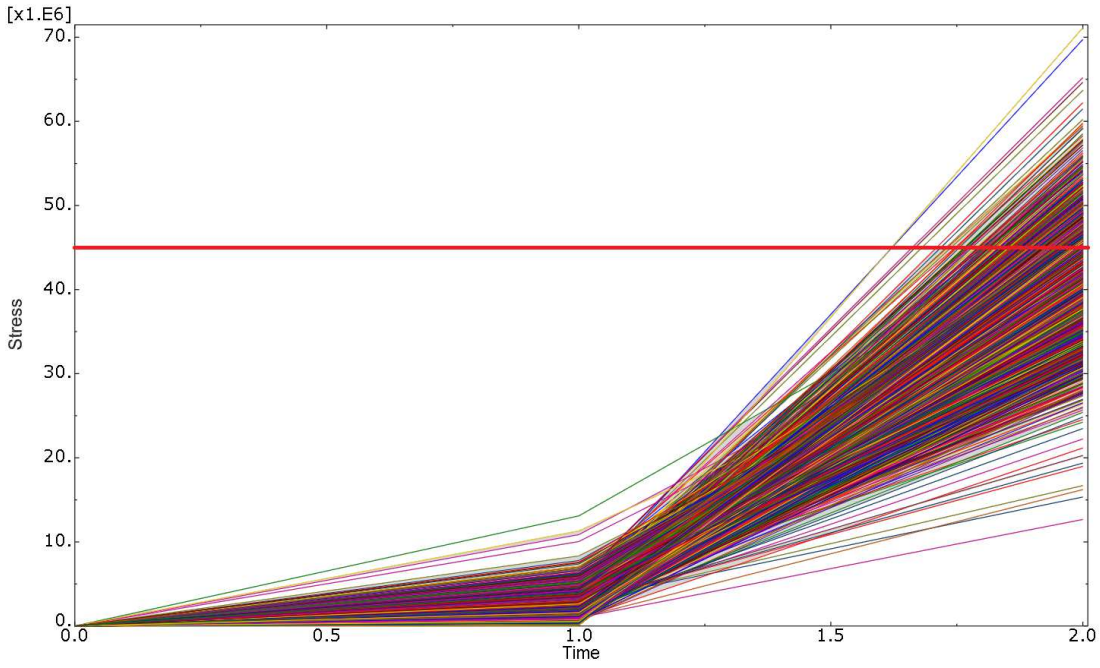

Figure 4.10: 1% strain with initial stresses

Chapter 5

Concluding remarks

An application to read and apply the TTSP to relaxation modulus data obtained from DMTA analysis was developed. The results obtained enable to assess the methodology developed to the problem under analysis. Nevertheless, the results obtained also seem to fog some of the conclusion which could be withdrawn mainly in what concerns the quantitative analysis. The latter may be due to experimental cumulative errors on a micropart or process numerical simulation inadequacies on the microscale. Both require further investigation.

Difficulties related to the correct mounting and geometry of the micropart should be referred, since the first specimens results were inconclusive. After noting the possible influence of the testing specimen geometry in results and using a new geometry, ABS was assessed as a thermorhelogically simple polymer through the Cole-Cole and van Gurp Palmen methodologies. Master curves were then obtained, by applying TTSP to ABS with the same horizontal shift values for all the properties. However, superposition in storage modulus revealed to be more complicated, which can suggest that the cause for this is purely elastic, and therefore appears to show up predominantly on storage modulus. The application includes two different methodologies and the second yielded the best results. Also, parameters for equations that allows to calculate shift factors were obtained.

Once obtained the master curves, a viscoelastic model was created. This model served to define the material behaviour when assessing the influence of residual stresses in parts obtained via micro injection moulding. The influence of residual stresses due to processing on final stresses was assessed through numerical comparison with an equal part but without initial stresses. This comparison revealed that initial stresses are very important even if their isolated value is low.

Also the viscoelasticity limit of 1% was analysed. This analysis revealed that this value might have to be reviewed for applications at the microscale.

Despite that a complete methodology for assessing numerical residual stresses influence on micro-parts behaviour when in service was proposed.

Figure 5.1 shows briefly the adopted methodology in a very general form:

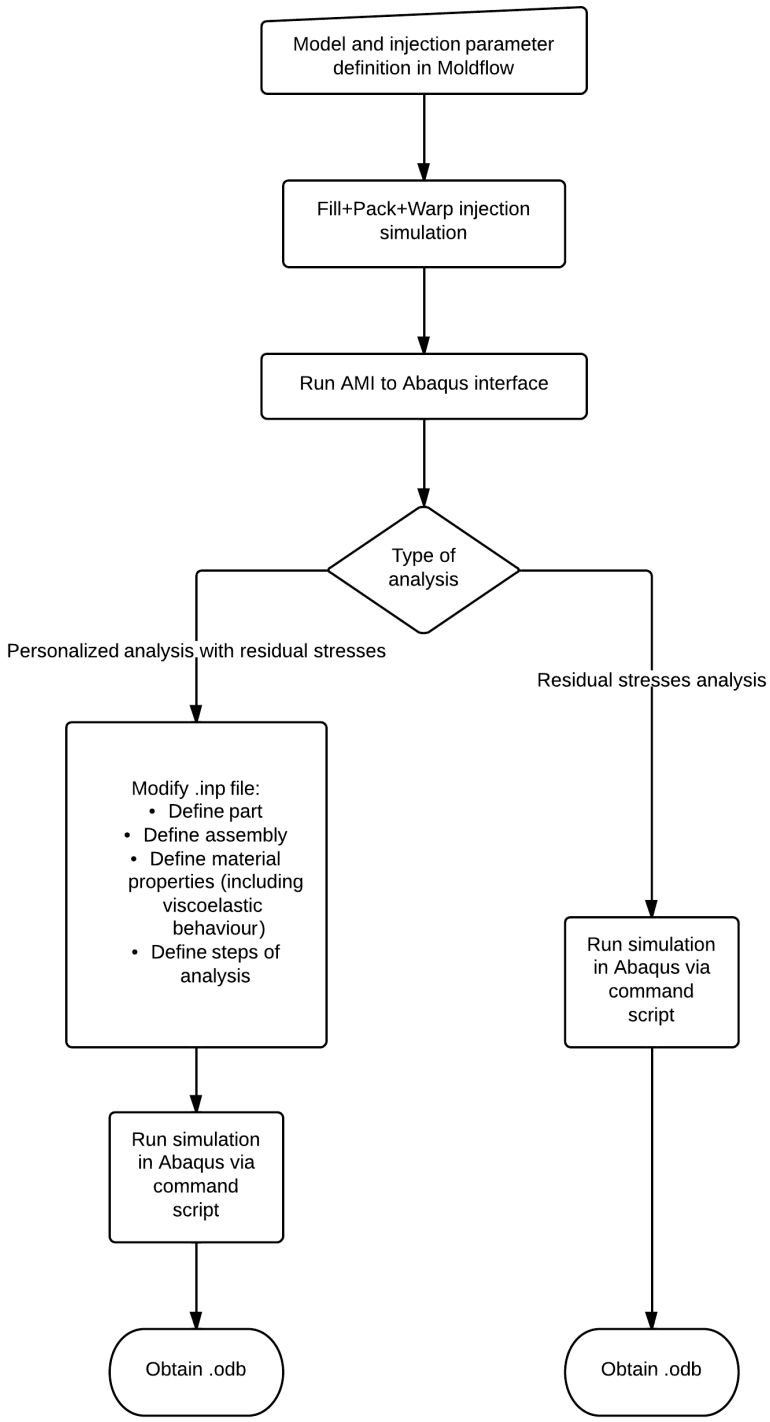

Figure 5.1: Methodoly for injection moulded parts rheological and structural analysis

Future work

Some aspects of the proposed analysis require further investigation. Therefore, some tests should be re-done to confirm or correct obtained data and some others should be

made. Some suggestions to future work may be:

Since few DMTA tests were performed, new test should be done in order to:

- evaluate elastic modulus at low temperatures and higher frequencies and compare the obtained value with the manufacturer stated value for elastic modulus;
- evaluate the repeatability and reliability of the obtained data;
- evaluate the necessity to develop DMTA machines oriented to micro-scale injected parts;
- perform temperature dependent measurements at a fixed frequency of $1Hz$ to observe secondary; transitions that may be occurring and influencing storage modulus superposition;
- perform relaxation tests in the referred conditions and compare them with the obtained from numerical simulations. This procedure may allow one to validate the viscoelastic model created with TTSP since if the model is representative of the polymer, stresses magnitudes may be similar;
- perform time-dependent measurements to evaluate possible physical changes and thermal instability due to the time temperature relation [14];
- perform tensile tests to distinguish polymer's elastic and non-elastic zone. From this test, limits of linear viscoelasticity for micro-injected parts may be evaluated.

References

[1] http://www.cefamol.pt/cefamol/pt/Cefamol_IndustriaMoldes in 27-02-2012.

[2] http://microinjecaodetermoplasticos.blogspot.pt/ in 27-02-2012.

[3] http://www.hindawi.com/journals/ijs/2010/206362/fig2/ in 05-03-2012.

[4] http://www.tangram.co.uk/TI-Polymer-Shrinkage_in_plastics.html in 15-05-2013.

[5] Abaqus 6.10 Analysis User's Manual-Dassault Systemes, 2010.

[6] M. F. F. de Moura, A.B. de Morais, and A.G. Magalhães. *Materiais Compósitos. Materiais, fabrico e comportamento mecânico.* Publindústria, 2005, 2005.

[7] J. Dealy and D Plazek. Time-Temperature Superposition - A Users Guide. *Rheology Bulletin*, 78:16–31.

[8] John M. Dealy and K.F. Wissbrun. *Melt Rheology and Its Role in Plastics Processing: Theory and Applications.* Kluwer Academic Publishers, 1990.

[9] Witold Edited by Brostow and Roger D. Corneliussen, editors. *Failure of Plastics.* Hanser Publishers, 1986.

[10] John D Ferry. *Viscoelastic properties of polymers, 3rd edition.* John Wiley & Sons, Ltd, 1980.

[11] M. Gergesova, B. Zupancic, I. Saprunov, and I. Emri. The closed form t-T-P shifting (CFS) algorithm. *Journal of Rheology*, 55, 2011.

[12] R. M. Guedes, Marina Gomes, and J. a. Simões. DMTA analysis for long-term mechanical behaviour prediction of PMMA-based bone cements. *Journal of Biomaterials Science, Polymer Edition*, 17(10):1173–1189, January 2006.

[13] Rui Miranda Guedes. A viscoelastic model for a biomedical ultra-high molecular weight polyethylene using the timetemperature superposition principle. *Polymer Testing*, 30(3):294–302, May 2011.

[14] Marnix Van Gurp and Jo Palmen. Time-temperature superposition for polymeric blends. *Rheology Bulletin*, 67:5–8, 1998.

[15] P H P Macaubas and N R Demarquette. Time-Temperature Superposition Principle Applicability for Blends Formed of Immiscible Polymers. *Polymer Engineering and Science*, 42(7):1509–1519, 2002.

[16] Computational Mechanics. *Computational Viscoelasticity*.

[17] Kevin P Menard and Kevin Peter. *DYNAMIC MECHANICAL ANALYSIS A Practical Introduction*. CRC Press, 1999.

[18] E. Miller. *Introduction to Plastics and Composites: Mechanical Properties and Engineering Applications (Mechanical Engineering Series)*. CRC Press, 1995.

[19] Rui A. S. Moreira. *Vibrações, Modelação e análise de tratamentos viscoelásticos multi-camada para controlo passivo de vibrações*. PhD thesis, FEUP, 2004.

[20] Dominick V. Rosato, Donald V. Rosato, and Marlene G. Rosato. *Injection Molding Handbook 3rd edition*. Kluwer Academic Publishers, 2000.

[21] Montgomery T Shaw and William J Macknight. *Introduction to Polymer Viscoelasticity Third Edition*. John Wiley & Sons, Ltd, 2005.

[22] Mehdi Tajvidi, Robert H. Falk, and John C. Hermanson. Time-temperature superposition principle applied to a kenaf-fiber/high-density polyethylene composite. *Journal of Applied Polymer Science*, 97(5):1995–2004, September 2005.

[23] Goga Vladimír. Testing and Application of New Phenomenological. pages 1–11, 2013.

[24] I. M. Ward and J. Sweeney. *The mechanical properties of solid polymers, second edition*. John Wiley & Sons, Ltd, 2004.

[25] T V Zhil'tsova, J A Ferreira, R A F Valente, and M S A Oliveira. Assessment of Residual Stresses in the in Mould Insert Moulded Parts. 2007.

[26] T V Zhiltsova, M S A Oliveira, J C Vasco, and A S Pouzada. Influence of mesh discretization on the prediction of polymer flow behaviour in micro microcavities. 2011(April):18–20, 2011.